

A Thermal Gradient Approach for the Quasi-Harmonic Approximation and its Application to Improved Treatment of Anisotropic Expansion

Nathan S. Abraham and Michael R. Shirts*

Department of Chemical and Biological Engineering, University of Colorado Boulder, Boulder, CO 80309, USA

E-mail: michael.shirts@colorado.edu

Abstract

We present a novel approach to efficiently implement thermal expansion in the quasi-harmonic approximation (QHA) for both isotropic and more importantly, anisotropic expansion. In this approach, we rapidly determine a crystal’s equilibrium volume and shape at a given temperature by integrating along the gradient of expansion from zero Kelvin up to the desired temperature. We compare our approach to previous isotropic methods that rely on a brute-force grid search to determine the free energy minimum, which is infeasible to carry out for anisotropic expansion, as well as quasi-anisotropic approaches that take into account the contributions to anisotropic expansion from the lattice energy. We compare these methods for experimentally known polymorphs of piracetam and resorcinol and show that both isotropic methods agree to within error up to 300 K. Using the Grüneisen parameter causes up to 0.04 kcal/mol deviation in the Gibbs free energy, but for polymorph free energy differences there is a cancellation in error with all isotropic methods within 0.025 kcal/mol at 300 K.

Anisotropic expansion allows the crystals to relax into lattice geometries 0.01–0.23 kcal/mol lower in energy at 300 K relative to isotropic expansion. For polymorph free energy differ-

ences all QHA methods produced results within 0.02 kcal/mol of each other for resorcinol and 0.12 kcal/mol for piracetam, the two molecules tested here, demonstrating a cancellation of error for isotropic methods.

We also find that when expanding in more than a single volume variable, there is a non-negligible rate of failure of the basic approximations of QHA. Specifically, while expanding into new harmonic modes as the box vectors are increased, the system often falls into alternate, structurally distinct harmonic modes unrelated by continuous deformation from the original harmonic mode.

1 Introduction

Computational screening of organic solid materials has garnered significant additional interest within the past decade. The most notable contributions to this field have emerged through crystal structure prediction (CSP) algorithms. CSPs provide a way to find potential polymorphs that can vary significantly in properties from previously known structures.^{1–5} CSPs use a combination of exhaustive searches of crystal lattice packings and carefully tuned force fields adapted to solid state organic molecules to accurately predict stable crystal conformations. They have shown significant progress over the

last decade in identifying experimentally observed polymorphs, or at least ranking experimental structures relatively highly among many alternate structures, in a series of blind prediction challenges. Over the years, the predictions have been moving towards crystals composed of larger and more flexible molecules.⁶⁻¹¹

A current limitation in CSP approaches is the static treatment of the crystal.¹² Typically, CSPs rely on the lattice energy to rank predicted structures, which excludes any dynamic behavior in the crystal. One can improve the CSP estimate by adding the entropy due to lattice vibrations. In the simplest lattice dynamic model, the harmonic approximation (HA), we assume that the crystal vibrates as a set of harmonic oscillators, providing a harmonic approximation to the Gibbs free energy:

$$G(T) = \min_{\mathbf{x}} (U(V_0, \mathbf{x})) + A_v(V_0, T) + PV \quad (1)$$

In the HA, we assume the Gibbs free energy (G) is a function of temperature and is a simple sum of the lattice energy (U) and the temperature dependent harmonic vibrational free energy (A_v) of the given structure. In eq. 1, T is the temperature of interest, $\min_{\mathbf{x}} (U(V_0, \mathbf{x}))$ is the lattice energy (U) at the lattice minimum volume (V_0) and geometry minimized coordinates (\mathbf{x}), and P is the pressure. Nyman and Day showed that 9% of 500 pairs of small molecule polymorphs re-ranked between 0 and 300 K.¹³ This percentage is still significant, considering that thermal expansion of the crystal is neglected in this estimate.

To most accurately model crystals, one should include the thermal expansion of a crystal. Crystals expand with temperature, increasing the total potential energy of the crystal, but also increasing the entropy. To improve upon the lattice dynamic model, we can use the quasi-harmonic approximation (QHA), which corrects eq. 1 by treating it as an argument-minimization of the volume:

$$G(T) = \min_V f(V, T) \quad (2)$$

$$f(V, T) = \min_{\mathbf{x}} (U(V, \mathbf{x})) + A_v(V, T) + PV \quad (3)$$

While being more computationally demanding, this model provides a more realistic depiction of the way solid materials behave, especially at low temperatures where anharmonic vibrations are negligible. As a follow-up study to their previous work on harmonic analysis of a large set of polymorphs, Nyman and Day re-evaluated the same structures using QHA, and found that 21% of the crystal structures re-ranked from 0 K to their melting temperature,¹⁴ further demonstrating that more accurate representation of finite temperature crystals can be important.

In eq. 3 it is most straightforward and most common to perform the argument minimization with an isotropic constraint on the lattice volume, holding lattice vectors proportional and angles fixed. While isotropic QHA methods have worked for small organic crystals, Heit et al. discuss how these predictions could be improved by considering anisotropic expansion.¹⁵ In particular, anisotropic treatments are expected to become more prevalent for larger molecules or crystal structures that are inherently layered,¹⁶⁻²⁰ which is characteristic of many potential drug candidates or for use in organic semiconductors.

In a recent study, we examined the Gibbs free energy differences as a function of temperature between polymorphs of 12 small organic molecules with both molecular dynamics (MD) and QHA using isotropic expansion. We found that for the small, rigid, ordered crystals QHA and MD agreed within < 0.07 kcal/mol, whereas for the larger, flexible molecules or disordered crystals QHA deviated up to 0.37 kcal/mol from MD at 300 K. Because we were using an isotropic thermal expansion model for QHA we could not determine if the deviations between the QHA and MD were due to anharmonic motions, neglected in the QHA, or due to anisotropic thermal expansion. While MD showed that all 24 crystals exhibited some level of anisotropy during thermal expansion, the degree of anisotropy was greater for those systems in which QHA and MD deviated > 0.1 kcal/mol for polymorph free energy differences,²¹ motivating a closer look at the validity of the isotropic expansion approximation.

The standard approach for performing isotropic QHA is not directly amenable to a fully anisotropic free energy minimization. This standard approach requires a stepwise expansion of the lattice minimum structure to a set of new volumes, V_i , and re-minimizing the coordinates for each new volume. For each of these volumes, V_i , the harmonic approximation is calculated at each volume. At each temperature of interest, we then determine which of these HA calculations corresponds to the volume that minimizes G .²² We describe the procedure in more detail below. In theory, this approach could be applied to anisotropic expansion by varying all six box vector parameters, forming a large grid of lattice structures of different shapes and sizes.^{23,24} However, if we consider all six dimensions of anisotropic expansion, this approach scales with N^6 where N is the number of grid steps in each dimension. To converge on the true thermodynamic minimum the steps between expansions must be small, which is particularly problematic with scaling to the 6th power in the number of steps. One could fit some multidimensional function to a sparser grid, but there are no existing explicitly anisotropic equations of state, and other multidimensional splines are complex and may not converge similarly in differently behaving systems.

There have been important recent developments towards the inclusion of anisotropy in QHA calculations that attempt to get around these scaling problems. Erba et al. developed an approach that performs a stepwise expansion of the crystal lattice,^{25,26} but also includes an additional step where the compressed and expanded structures are energy minimized at the fixed expanded volume. To avoid too fine a grid of expansion and compression, the lattice energy is fit to an equation of state (in volume alone) and the vibrational frequencies, determined at these optimized structures, are fit with a polynomial (again in volume). With these two equations, the properties using eq. 3 can quickly be fit at any temperature or pressure, assuming the EoS is sufficiently accurate. This approach has been used in conjunction with *ab initio* techniques for a number of materials and

organic crystals, which has shown notable success matching experimental results up to high temperatures and pressures.²⁷⁻³¹ However, this approach performs the cell optimization based on the lattice energy alone, meaning the lattice geometry will not be at free energy minimum for that volume.

A nearly equivalent variation of this approach performs lattice minimization at a number of different increased and decreased pressures.³² Similar to Erba’s method, these (U, V) pairs, which implicitly include anisotropic expansion due to the lattice energy, are fit to an equation of state. These structures are minimum lattice energy structures at their volume; the only difference to the direct volume-constrained minimization is that these structures are likely not at uniform volume intervals, as the pressure is specified, not the volume.

Other options to employ anisotropic expansion for QHA, but most have drawbacks due to expense or are not at the true quasi-harmonic minimum. Some approaches use prior experimental knowledge,³³ which are ineffective for crystal structure predictions where high temperature lattice geometries are unknown. Alternatively, one could directly optimize the free energy with respect to all lattice parameters at each temperature,^{34,35} however, this requires a full nonlinear optimization of the sum of the lattice energy and the vibrational energy at each state point of interest, which typically involves a number of approximation for the vibrational energy.³⁴ This approach results in significant additional computational work, often requiring new derivations depending on the energy model used, which cannot be reused between state points without further approximation.

In this paper, we present a new way to efficiently compute the free energies of crystalline solids in the QHA for both isotropic and anisotropic thermal expansion based on estimating the gradient of thermal expansion. By computing the gradient of thermal expansion we are only limited by the numerical integration used and inherent failures in the QHA, which we will discuss in this paper. We compare our method to the stepwise approach for isotropic QHA and what has been referred to³²

as the “quasi-anisotropic” method of Erba and others.^{25,32,36} We examine how the free energies, the free energy differences between polymorphs, and the crystals geometries vary across the different methods. We also show how those thermodynamic properties vary when using the Grüneisen parameter to account for changes in the crystals vibrational spectra.

2 Theory

2.1 Harmonic Approximation

In the simplest lattice dynamic model, the harmonic approximation (HA), we assume that thermal expansion is negligible. The Gibbs free energy for HA is shown in eq. 1, where $\min_{\mathbf{x}}(U(V_0, \mathbf{x}))$ is the minimum of the internal energy at the crystal lattice minimum energy volume (V_0). The vibrational free energy, $A_v(V, T)$, is calculated as:

$$A_v(V, T) = \sum_k \frac{1}{\beta} \ln(\beta \hbar \omega_k(V)) \quad (4)$$

Where β is $(k_B T)^{-1}$ and $\omega_k(V)$ is the vibrational frequency of the k^{th} vibrational mode. Since the kinetic energy will be the same between polymorphs, we can simply use the potential energy instead of the total energy when examining the free energy difference between polymorphs. Note that the above formula is the classical approximation, though the approach presented here will be equally valid for the quantum harmonic oscillator formula.

2.2 Quasi-Harmonic Approximation

The quasi-harmonic approximation (QHA) more accurately captures entropic effects compared to HA by accounting for the entropic effects caused by thermal expansion. There are two ways to account for thermal expansion: isotropic and anisotropic. Isotropic thermal expansion assumes that 1) the lattice vectors remain proportional for all volumes and 2) that the lattice angles remain fixed. Isotropic

expansion is a computationally fast approximation to the true thermal expansion, and has been shown to work well for number of materials,^{15,22,37} but can constrain the crystal to the wrong lattice geometry at high temperatures for materials that expand anisotropically.^{38,39} In isotropic QHA, we calculate the minimum of the harmonic approximation over all volumes at a given temperature T . At $T = 0$, this will coincide with the harmonic approximation, but at $T > 0$ QHA will minimize G to a lower free energy minimum and larger volume.

In contrast, anisotropic expansion allows the 6 lattice parameters to change with no constraints. This is a more accurate model to describe thermal expansion, since most crystals exhibit some level of anisotropy. For this more accurate expansion model, we must minimize the argument over the crystal lattice tensor \mathbf{C} , which defines the box shape of a single unit cell:

$$\mathbf{C} = \begin{bmatrix} C_1 & C_4 & C_5 \\ 0 & C_2 & C_6 \\ 0 & 0 & C_3 \end{bmatrix} \quad (5)$$

As the energy of the crystal is a function of six lattice parameters, C_i for $i = 1, 2, \dots, 6$, not simply the volume alone.

$$G(T) = \min_{\mathbf{C}} f(\mathbf{C}, T) \quad (6)$$

$$f(\mathbf{C}, T) = \min_x (U(\mathbf{C}, x)) + A_v(\mathbf{C}, T) + PV(\mathbf{C}) \quad (7)$$

Full anisotropic expansion is difficult to carry out, because it requires optimization of a complicated argument in a substantially larger space.

2.3 Grüneisen Parameter

The vibrational spectra of the crystal changes as the strains are applied to the system, which must be accounted for in QHA. There are two options to compute ω_k for all values of \mathbf{C} . The first is to compute the mass-weighted Hessian for every structure with a unique lattice tensor \mathbf{C} , which is the most expensive step in the approximation. The second option is to assume that the changes in ω_k are proportional to the strains applied to the crystal, which is described

by the Grüneisen parameter. This approach is a standard technique used to speed up lattice dynamics calculations.^{15,22,40,41}

2.3.1 Isotropic Grüneisen Parameter

For isotropic thermal expansion, the Grüneisen parameter of a particular mode is the proportional change between that vibrational frequency and the lattice volume. To calculate this and minimize rounding error, we take the alternative formulation:

$$\frac{\partial V}{V} = -\frac{1}{\gamma_k} \frac{\partial \omega_k(V)}{\omega_k(V)} \quad (8)$$

Where again V is the isotropic volume, $\omega_k(V)$ is the vibrational frequency of the k^{th} mode at V , and γ_k is the Grüneisen parameter of the k^{th} mode.

By computing the derivatives of the log quantities by forward finite difference and rearranging eq. 8 we get eq. 9. We use the forward difference approach rather than the central difference approach because we require the 0 K vibrational spectra in any case, so computing a central difference will be at least 50% more expensive. Eq. 8 can be integrated to get eq. 10 and the solution from eq. 9 can be used to determine the k^{th} vibrational frequency at any subsequent isotropically expanded structure.

$$\gamma_k = -\frac{\ln(\omega_k(V + \Delta V)) - \ln(\omega_k(V))}{\ln(1 + \frac{\Delta V}{V})} \quad (9)$$

$$\omega_k(V + \Delta V) = \omega_k(V) \left(1 + \frac{\Delta V}{V}\right)^{-\gamma_k} \quad (10)$$

Where $\omega_k(V)$ is the k^{th} vibrational frequency for the lattice minimum structure, V is the lattice minimum volume, $V + \Delta V$ is the volume of the isotropically expanded structure, and $\omega_k(V + \Delta V)$ is the k^{th} vibrational frequency for the expanded structure.

2.3.2 Anisotropic Grüneisen Parameter

We can also assume that the change in relative vibrational frequencies is a linear combination of changes in each relative box vector, not just the volume itself, resulting in six

anisotropic Grüneisen parameters. To develop the formalism of inclusion of anisotropic expansion, we present the formalism from Choy et al.⁴² Eq. 11 describes the proportionality of a strain (η_i) placed on the lattice on the k^{th} vibrational frequency. Here η_i is one of the six principle strains on the crystal lattice matrix, $i = 1, 2, \dots, 6$.

$$(\partial \eta_i)_{\eta_j \neq \eta_i} = -\frac{(\partial \omega_k)_{\eta_j \neq \eta_i}}{\omega_k \gamma_{k,i}} \quad (11)$$

Similarly to the isotropic case, eq. 11 can be re-arranged and solved numerically for the six different strains shown in eq. 12.

$$\gamma_{k,i} = -\frac{\ln(\omega_k(\eta_i)) - \ln(\omega_{k,0})}{\eta_i} \quad (12)$$

If we integrate eq. 11 and use the solution from eq. 12, then the change in the k^{th} vibrational frequency due to strain η_i can be described by eq. 13, where $\omega_k(\eta_i)$ is the k^{th} vibrational frequency for the crystal under strain η_i , $\omega_{k,0}$ is the k^{th} vibrational frequency of the lattice structure, and $\gamma_{k,i}$ is the Grüneisen for the k^{th} mode due to strain η_i .

$$\omega_k(\eta_i) = \omega_{k,0} \exp(-\eta_i \gamma_{k,i}) \quad (13)$$

Eq. 13 can be used in a linear combination of all six strains on the system to predict the vibrational spectra due to any lattice strain.

$$\omega_k(\eta_{1,2,\dots,6}) = \omega_{k,0} \exp\left(\sum_{i=1}^6 -\eta_i \gamma_{k,i}\right) \quad (14)$$

To compute the six principle strains placed on the crystal during thermal expansion requires us to relate the crystal lattice tensor to strain. The six principle strains make up the strain tensor as:

$$\boldsymbol{\eta} = \begin{bmatrix} \eta_1 & \eta_4 & \eta_5 \\ \eta_4 & \eta_2 & \eta_6 \\ \eta_5 & \eta_6 & \eta_3 \end{bmatrix} \quad (15)$$

For η_i , $i = 1, 2$ and 3 are normal strains and $i = 4, 5$ and 6 are shear strains, which are applied symmetrically. By assuming that the crystals are strained by small amounts and that

angular momentum is conserved we can relate the lattice minimum crystal tensor (\mathbf{C}_0) to a new expanded tensor (\mathbf{C}) under strain $\boldsymbol{\eta}$, as:

$$\mathbf{C} = \mathbf{C}_0 (\mathbf{I} + \boldsymbol{\eta}) \quad (16)$$

Re-arranging to determine the strain, we can compute the strain placed on the reference crystal, \mathbf{C}_0 , to produce some new crystal tensor, \mathbf{C} .

$$\boldsymbol{\eta} = \mathbf{C}\mathbf{C}_0^{-1} - \mathbf{I} \quad (17)$$

There is a artificial rotation caused in the computation of the strain in eq. 17 due to the representation of the crystal tensor. Since we are dealing with bulk crystals, any rotational strain computed between two sets of lattice vectors will not correspond to a change in energy. Further discussion of the rotational strain and how we remove it to compute $\boldsymbol{\eta}$ as a symmetric tensor can be found in the Supporting Information (Section 14).

Knowing the applied strain relative to the reference structure and the set of Grüneisen parameters we can approximate the vibrational spectra of any crystal strained from the reference point by solving eq. 14.

2.4 Stepwise Thermal Expansion

The standard approach for performing isotropic QHA works reasonably well for isotropic expansion, but is too inefficient for anisotropic expansion. Typically, the crystal lattice structure would be expanded and compressed to create a subset of structures that could be described by an array of isotropic volumes V_i . The vibrational spectra of each structure would be computed, allowing us to perform a harmonic approximation on each structure. At a given temperature, the isotropic volume, V_i , that minimizes the Gibbs free energy would be used to describe the system at T . This method allows us to perform QHA in a brute force manner for isotropic expansion, but becomes infeasible when considering anisotropic thermal expansion, which would require either a 6D grid search. A detailed description of stepwise isotropic QHA can be found in section 3.1.

2.5 A New Approach: The Gradient Thermal Expansion

We wish to determine exactly how the structure expands with temperature to make isotropic expansion more efficient and provide a more suitable way to perform anisotropic expansion. We present an approach by Gould et al.⁴³ to solve argument min- or maximization problems, and apply this method to determine the rate of thermal expansion of organic crystals. Eq. 18 is a general minimization problem, which can be seen to be of the same class of problem as the equations for the QHA Gibbs free energy in eq. 3 and eq. 7.

$$g(t) = \min_x f(x, t) \quad (18)$$

Where the solution to $g(t)$ is the equal to the minimum of $f(x, t)$ with respect to x . The gradient of x as a function of t , in eq. 19, can be computed as (see Gould et al.):⁴³

$$\frac{\partial x}{\partial t} = - \frac{\frac{\partial^2 g}{\partial x \partial t}}{\frac{\partial^2 g}{\partial x^2}} \quad (19)$$

If we can compute these partial derivatives, then we can use the gradient $\frac{dx}{dt}$ to solve the resulting ordinary differential equation for $x(t)$. Eq. 19 can be applied to single or multidimensional problems, which we outline for both isotropic and anisotropic expansion. In these cases, the variable t in eq. 18 is the temperature T , and x in eq. 18 is either the volume V or the components of the crystal tensor \mathbf{C} .

2.5.1 Gradient Isotropic Thermal Expansion

We can easily apply eq. 18 to eq. 3 to obtain a thermal gradient approach to calculating the expansion needed for QHA expansions, obtaining for the volume:

$$\frac{\partial V}{\partial T} = - \frac{\frac{\partial^2 G}{\partial V \partial T}}{\frac{\partial^2 G}{\partial V^2}} = \frac{\partial S}{\partial V} \quad (20)$$

We use the additional simplification of replacing the temperature derivative of G with $-S$, as S can be easily calculated analytically once G

is calculated. The analytical solution of S is derived from eq. 4 and shown in eq. 21.

$$S(V, T) = \sum_k k_B (1 - \ln(\beta \hbar \omega_k(V))) \quad (21)$$

With the thermal gradient calculated in eq. 20, we can determine how the minimum energy volume changes with temperature by using any standard algorithm for ordinary differential equations; in this paper, we use the 4th order Runge-Kutta approach.

2.5.2 Gradient Anisotropic Thermal Expansion

Eq. 7 presents the thermal expansion gradient for anisotropic expansion; eq. 23 shows this solution using the thermal expansion approach.

$$\frac{\partial \mathbf{C}}{\partial T} = - \left(\frac{\partial^2 G}{\partial \mathbf{C}^2} \right)^{-1} \frac{\partial^2 G}{\partial \mathbf{C} \partial T} \quad (22)$$

$$= \left(\frac{\partial^2 G}{\partial \mathbf{C}^2} \right)^{-1} \frac{\partial S}{\partial \mathbf{C}} \quad (23)$$

Here, \mathbf{C} is the array of the three diagonal and three off diagonal elements, all of which describe the orientation of the lattice vectors:

$$\mathbf{C} = [C_1 \ C_2 \ C_3 \ C_4 \ C_5 \ C_6]^T \quad (24)$$

Given the dimensions of \mathbf{C} , the left hand side of eq. 23 and the second term on the right hand side are length-six vectors. The first term on the right hand side is a 6×6 matrix. Similar to the isotropic case, the anisotropic gradients are solved using a central finite difference approach.

In some cases, parts of $\frac{\partial^2 G}{\partial \mathbf{C}^2}$ due to a given lattice vector may be inherently zero, which will make the matrix singular. We therefore solve the thermal gradient using the implicit formulation in eq. 25.

$$\left(\frac{\partial^2 G}{\partial \mathbf{C}^2} \right) \frac{\partial \mathbf{C}}{\partial T} = \frac{\partial S}{\partial \mathbf{C}} \quad (25)$$

Using the thermal gradient calculated in eq. 25, we can determine how the minimum energy volume changes with temperature by using any standard algorithm for, now, coupled first

order ordinary differential equations; in this paper, we again use the Runge-Kutta approach.

2.6 Constrained Anisotropic Expansion

A full six-dimensional search for anisotropic expansion is accurate, but is computational demanding. For the purpose of our study we also present three constrained versions of anisotropic expansion that may provide a more efficient search for the free energy minimum, and test to see how well they perform.

2.6.1 3-Dimensional Anisotropic Expansion

The primary factors in thermal expansion is elongation of the lattice vectors or diagonal elements of the crystal lattice tensor, \mathbf{C} . While the off-diagonals can change during thermal expansion, we noticed in our initial work that the greatest change is in the diagonal elements. To study the importance of the off-diagonal elements in QHA, we examine anisotropic expansion where the off-diagonal elements remain fixed. That is, the gradient of thermal expansion, $\frac{\partial C_i}{\partial T}$, will only be solved for elements $i = 1, 2, 3$ of the crystal lattice tensor and eq. 25 becomes an equation in a 3 dimensional vector of box lengths.

2.6.2 1-Dimensional Anisotropic Expansion

We also present a third option for anisotropic expansion that mimics the fixed expansion in isotropic expansion, but utilizes anisotropic thermal expansion ratios computed at 0 K. This approach is based on the same philosophy as the constant Grüneisen parameter approach, which assumes that changes over most of the temperature range of interest are linear extrapolations of the behaviors at $T = 0$ K, which anecdotally is a reasonable approximation. At the initial step of this variant of QHA, we determine the ratio in which values of C_i change due to thermal expansion. We do this by solving eq. 25 for the lattice minimum structure at 0 K to find

$\kappa_i = \left(\frac{\partial C_i}{\partial T}\right)_{T=0\text{ K}}$, introducing the variable κ_i as the derivative of C_i with respect to T at 0 K. Using the initial lattice structure, $\mathbf{C}(T = 0\text{ K})$, and the computed rate of thermal expansion, we can re-write C_i as a function of a scaling factor λ , shown in eq. 26.

$$C_i(\lambda) = C_i(\lambda = 0) + \kappa_i\lambda(T) \quad (26)$$

Where we parameterize λ such that $C_i(\lambda = 0) = C_i(T = 0\text{ K})$. More complicated parameterizations of $C_i(\lambda)$ can easily be defined, but we restrict this paper to the linear expansion given in eq. 26.

Similarly to isotropic and anisotropic thermal expansion, we can determine the thermal gradient of λ by solving eq. 27.

$$\frac{\partial \lambda}{\partial T} = \frac{\frac{\partial S}{\partial \lambda}}{\frac{\partial^2 G}{\partial \lambda^2}} \quad (27)$$

Eq. 26 is now a ordinary differential equation in λ . We can solve for $\lambda(T)$, which will give us the box vectors C_i that minimize the free energy subject to the constraint given by Eq.26.

2.6.3 Quasi-Anisotropic Expansion

Our last anisotropic approach has been presented in literature in several similar forms^{25,32} and provides an avenue to perform the stepwise thermal expansion approach while including some anisotropy within the crystal lattice. Similar to the stepwise approach, the crystal structure is compressed and expanded to several volume fractions around the lattice minimum structure; however, each compressed/expanded crystal structure is minimized at fixed volume find the minimum 0 K lattice geometry at that specified volume.

3 Methods

We compare the efficiency and accuracy of eleven lattice dynamic calculations using combinations of the procedures above. Eight of these are new approaches based on the thermal gradient approach. These methods, and the abbreviations are shown in Table 1.

3.1 Crystal Polymorph Systems Tested

We selected resorcinol and piracetam to test all eleven methods on, both of which were studied in our previous work.⁴⁴ The two systems were chosen because StepIso-QHA determined that the lattice vectors only changed by 1–2% from 0 to 300 K, but for MD, where anisotropy is considered, the lattice vectors change by -1–5%. Additionally, it was found that piracetam form I had a box angle change with increasing temperature, which cannot be observed with an isotropic thermal expansion model.

Stepwise Isotropic QHA (StepIso-QHA): For stepwise isotropic QHA,

1. the initial lattice minimum structure is expanded isotropically by a small volume fraction;
2. the new expanded system is geometry optimized;
3. steps 1 and 2 are repeated on the expanded structure; and
4. the process is continued until the crystal is expanded past the anticipated volume at the maximum temperature.

Computing the lattice energy of all expanded structures produces a lattice energy curve $U(V)$. The mass-weighted Hessian of each expanded structure is computed and diagonalized to provide $\omega_k(V_i)$, allowing the computation of a vibrational surface $A_v(V, T)$. At each temperature the lattice volume, that minimizes the Gibbs free energy is used to solve for $G(T)$ in eq. 3. A schematic of the stepwise approach is shown in fig. 2. For our work, we chose to compress and expand each crystal structure to volume fractions $((V + \Delta V)/V)$ of 0.99 and 1.08 respectively, which is sufficiently large for the crystals examined here. Intermediate volumes between 0.99 and 1.08 were evaluated at values of $\Delta V/V = 10^{-3}$. We discuss how the choice of $\Delta V/V$ effects the smoothness of $V(T)$ and $G(T)$ in the Supporting Information (Section 8).

While the result in fig. 2 is straightforward to calculate for isotropic expansion, it becomes

Table 1: The eleven methods tested in this paper categorized by the type of thermal expansion and the approach by which Hessians are estimated.

Methods Tested		
Expansion	Full Hessian	Grüneisen or Polynomial Fit
None	Harmonic approximation (HA)	
Isotropic	Stepwise isotropic QHA (StepIso-QHA)	Stepwise isotropic QHA assisted with the Grüneisen parameter (StepIso-QHA γ)
	Gradient isotropic QHA (GradIso-QHA)	Gradient isotropic QHA assisted with the Grüneisen parameter (GradIso-QHA γ)
Non-Isotropic	1-Dimensional Gradient anisotropic QHA (1D-GradAniso-QHA)	1-Dimensional Gradient anisotropic QHA assisted with the Grüneisen parameter (1D-GradAniso-QHA γ)
	3-Dimensional Gradient anisotropic QHA (3D-GradAniso-QHA)	3-Dimensional Gradient anisotropic QHA assisted with the Grüneisen parameter (3D-GradAniso-QHA γ)
	Unconstrained Gradient anisotropic QHA (GradAniso-QHA)	Unconstrained Gradient anisotropic QHA assisted with the Grüneisen parameter (GradAniso-QHA γ)
		Quasi-anisotropic QHA (QuasiAniso-QHA)

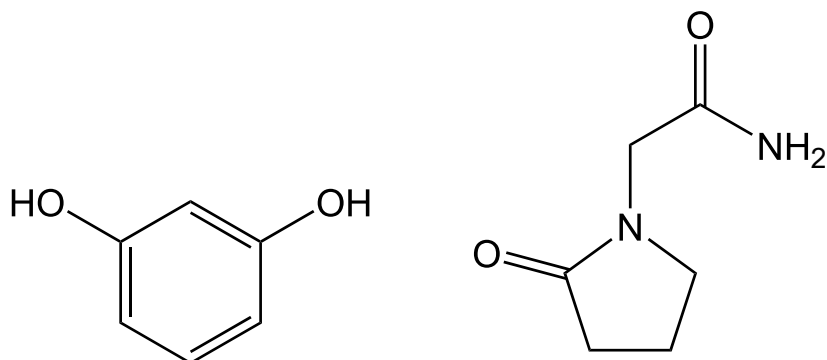


Figure 1: Polymorphic systems evaluated in this paper using variants of QHA are resorcinol (left) and piracetam (right).

considerably more expensive for anisotropic expansion. The one dimensional problem of isotropic expansion scales with the number,

N , of sampled points, $\{V_0, V_1, \dots, V_N\}$. For anisotropic expansion, the problem is now six dimensional, which will scale as N^6 in order to

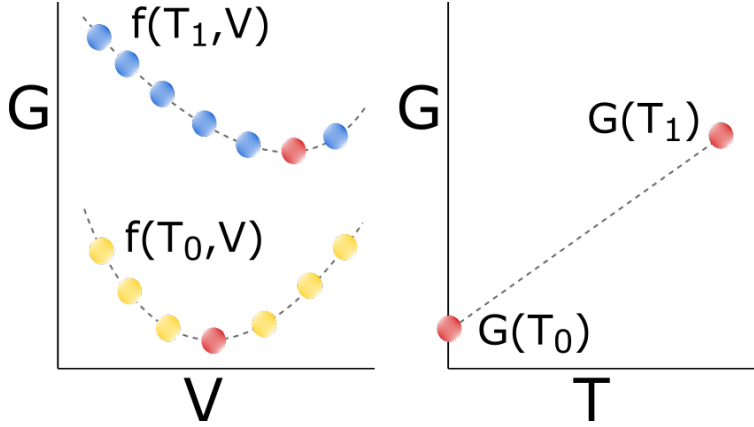


Figure 2: Schematic of stepwise isotropic QHA. The G vs. V plot (left) shows $f(V, T)$ at two temperatures, T_0 and T_1 . At T_0 the lowest energy structure, in red, is isotropically expanded and compressed, with each structures free energy computed $f(T_0, V)$ is formed. The free energy of each structure is re-evaluated at T_1 , generating $f(T_1, V)$. At each temperature i , the lowest free energy structure is chosen for each i by minimizing $f(T_i, V)$, and the free energy at T_i is set to this minimum, allowing the construction of $G(T)$ shown (right).

determine the minimum free energy structure for all six lattice parameters. While not every sample is required, as some can be ruled out as being too far from the minimum, we in general need some understanding of how the crystal expands before limiting the N^6 dimensional space to something more feasible.

Stepwise Isotropic QHA with the Grüneisen Parameter (StepIso-QHA γ): Similar to StepIso-QHA, stepwise isotropic QHA with the Grüneisen parameter involves isotropic expansion of the initial lattice minimum structure by a small steps to produce the same lattice energy curve in StepIso-QHA. Where StepIso-QHA and StepIso-QHA γ differ is the calculation of the vibrational spectra of every structure. StepIsoQHA γ circumvents multiple Hessian calculations by approximating changes in the vibrational spectra due to expansion by assuming the Grüneisen parameter, calculated using eq. 9, is independent of box volume, meaning it can be calculated using eq. 10. This significantly decreases the computational cost compared to StepIso-QHA.

Gradient Isotropic QHA (GradIso-QHA): Gradient QHA provides a more efficient way to calculate free energy curves and the gradient method can be easily performed for anisotropic expansion. Fig. 3 depicts how gradient isotropic

QHA works. At 0 K the gradient of thermal expansion is determined by isotropically expanding and compressing the lattice minimum structure to solve eq. 20.

Comparing figures 3 and 2 shows that a gradient approach requires only the structures local to the minimum at any given temperature, while the stepwise approach can require many more. We also note that the stepwise approach only produces a smooth $V(T)$ curve if there is minimal spacing between expanded structures, while the gradient approach only relies on the numerical method used. Since we do not have an analytical solution to eq. 20, we will need to solve for $\frac{\partial V}{\partial T}$ numerically. We implement a 4th order Runge-Kutta method to accurately determine the free energy curve across the entire temperature range.

The solution of $\frac{\partial V}{\partial T}$ is solved by computing $\frac{\partial S}{\partial V}$ and $\frac{\partial^2 G}{\partial V^2}$ with a central finite difference approach. The lattice minimum structure is isotropically expanded and compressed, the mass-weighted Hessian is computed and diagonalized for the vibrational spectra of all three structures, and the Gibbs free energy is evaluated to determine the numerical gradient. For GradIso-QHA we found that only three Runge-Kutta steps of 100 K are required to produce a visually smooth volume versus temperature

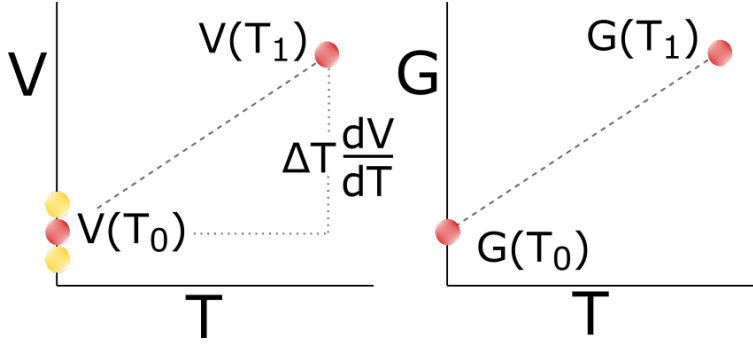


Figure 3: Schematic of gradient isotropic QHA. On the V vs. T plot (left) the known lattice minimum structure with volume $V(T_0)$ is shown along the y -axis as the red dot. To determine the gradient of expansion using finite differences, the structure is expanded and compressed, indicated by two yellow dots on the y -axis, and $\partial S/\partial V$ and $\partial^2 G/\partial V^2$ are estimated. With each structure’s Gibbs free energy and entropy, we can determine $\frac{\partial V}{\partial T}$ using eq. 20, and with a given temperature step, ΔT , the volume of the structure at T_1 can be computed with numerical integration. The structure at T_0 can be directly expanded to $V(T_1)$ and the free energy of the expanded structure can be computed to compute $G(T_1)$ (right).

curve up to 300 K. To solve for intermediate temperature points, we used a 3^{rd} order spline on the volume parameter, which uses the first Runge-Kutta gradient at T_i and T_{i+1} to determine $V(T)$ for $T_i \leq T \leq T_{i+1}$.⁴⁵ Further information on step sizes can be found in the Supporting Information (Section 10).

Gradient Isotropic QHA with the Grüneisen Parameter (GradIso-QHA γ): Gradient isotropic QHA with the Grüneisen Parameter uses the same local gradient approach as GradIso-QHA, with replacement of the calculation of the vibrational frequencies through the Hessian with the calculation using the Grüneisen parameter approximation. Before any gradients are calculated, the Grüneisen parameters are calculated using eq. 9. The local gradient is calculated the same way as in GradIso-QHA, except that instead of calculating the mass-weighted Hessian of the isotropically expanded structures, eq. 10 provides the new vibrational spectra.

Quasi-anisotropic QHA (QuasiAniso-QHA): Quasi-anisotropic QHA uses a similar methodology to that implemented in the CRYSTALS program³⁶ as well variants used by other researchers.³² The lattice minimum structure is first isotropically expanded and compressed to several volumes of interest. We then perform

a volume-constrained optimization of the lattice energy for each volume, and then fit the potential energy with an equation of state and a polynomial fit to each vibrational frequency. We then use the fitted functions of the energy and vibrational modes to minimize the Gibbs free energy at each temperature of interest.

For our work, we chose to compress and expand each crystal structure to volume fractions $((V + \Delta V)/V)$ of 0.99 and 1.05 respectively. Intermediate volumes between 0.99 and 1.05 were evaluated at values of $\Delta V/V = 10^{-2}$, which is an order of magnitude larger than StepIso-QHA since we are using a polynomial fit. We then perform a volume-constrained optimization of the lattice energy and fit the $U(V)$ with the Rose-Vinet equation of state. This optimization was implemented as a bounded constrained optimization in Python wrapped around TINKER energy call, more information can be found in the Supporting Information (Section 16). This is clearly not the fastest way to perform the optimization, but allowed us to perform the optimization without changing the underlying code base. The vibrational frequencies of all structures are computed and each frequency is fitted with a 3^{rd} order polynomial. We then use these these functions to determine the volume that minimizes the Gibbs free en-

ergy, eq. 7. We verified that constrained volume optimizations were at the correct minimum by using the method of Lagrange multipliers.

Gradient Anisotropic QHA (GradAniso-QHA): Modeling anisotropic expansion includes a greater number of variables to minimize along, making it computationally costly compared to isotropic expansion. We have therefore chosen to apply only the gradient method to anisotropic QHA because the step-wise approach, which would require enumeration of the points on a 6D grid would be too expensive. Gradient anisotropic QHA uses a similar approach as GradIso-QHA, except instead of determining the volumetric thermal gradient, we compute the gradient of the six lattice parameters. We solve $\frac{\partial C}{\partial T}$ in eq. 25 using a finite difference approach and apply a 4th order Runge-Kutta method to converge onto the structure that minimizes the Gibbs Free energy.

$\frac{\partial C}{\partial T}$ is computed from the solution of $\frac{\partial S}{\partial C_i}$ and $\frac{\partial^2 G}{\partial C_i^2}$ with a central finite difference approach. For each lattice parameter, the lattice minimum structure is expanded or compressed ($C_i \pm dC_i$) while holding the other lattice parameters constant. The altered structures are geometry optimized, the mass-weighted Hessian is computed and diagonalized for the vibrational spectra for all structures, and the Gibbs free energy is evaluated to determine the numerical gradient. In the case where the lattice minimum structure has a value of $C_i = 0$, we set $dC_i = 0$. Similar to GradIso-QHA, we found that three Runge-Kutta steps produced a structure at a free energy minimum for all temperature and intermediate steps were solved with a 3rd order spline. For further information regarding the choice of step sizes used in the finite difference, refer to the Supporting Information (Section 10).

Gradient Anisotropic QHA with the Grüneisen Parameter (GradAniso-QHA γ): Gradient anisotropic QHA with the Grüneisen Parameter uses the same local gradient approach as GradAniso-QHA with the replacement of the Grüneisen parameter to approximate the vibrational spectra of all expanded structures.

3D-Gradient Anisotropic QHA (3D-GradAniso-

QHA): Three dimensional gradient anisotropic QHA follows the same approach as GradAniso-QHA, except components $i = 4, 5, 6$ for $\frac{\partial C_i}{\partial T}$ are zero. This means that in eq. 25, $\frac{\partial C}{\partial T}$ and $\frac{\partial S}{\partial C}$ are three component vectors and $\frac{\partial^2 G}{\partial C^2}$ is reduced to a 3 \times 3 matrix. We then integrate up with temperature by taking Runge-Kutta step sizes of 100 K up to 300 K and determine intermediate points with a 3rd order spline, which is the same as what was done in isotropic and unconstrained anisotropic expansion.

3D-Gradient Anisotropic QHA with the Grüneisen Parameter (3D-GradAniso-QHA γ): Three dimensional gradient anisotropic QHA with the Grüneisen Parameter uses the same local-gradient approach as 3D-GradAniso-QHA with the addition of the Grüneisen parameter to approximate the vibrational spectra of all expanded structures.

1D-Gradient Anisotropic QHA (1D-GradAniso-QHA): One dimensional gradient anisotropic QHA allows us to capture anisotropic expansion, with little additional computational cost compared to GradIso-QHA. With the lattice minimum structure, we compute $\frac{\partial C}{\partial T}$ at 0 K, which provides a fixed ratio κ_i for how the lattice parameters can change relative to each other with temperature. In eq. 26, $C_i(\lambda = 0)$ at 0 K and $\frac{\partial \lambda}{\partial T}$ can be computed to determine how λ changes with temperature.

We first compute $(\frac{\partial C_i}{\partial T})_T = 0 K$ in the same way performed in GradAniso-QHA, but this is performed only on the lattice minimum structure to get the values of κ_i . The solution of $\frac{\partial \lambda}{\partial T}$ is solved by computing $\frac{\partial S}{\partial \lambda}$ and $\frac{\partial^2 G}{\partial \lambda^2}$ with a central finite difference approach. The lattice minimum structure is expanded and compressed by changing λ in eq. 26 by $\pm d\lambda$, the mass-weighted Hessian is computed and diagonalized for the vibrational spectra of all three structures, and the Gibbs free energy is evaluated to determine the numerical gradient. We then integrate up with temperature by taking Runge-Kutta step sizes of 100 K up to 300 K and determine intermediate points with a 3rd order spline, which is the same as is done in isotropic and unconstrained anisotropic expansion.

1D-Gradient Anisotropic QHA with the

Grüneisen Parameter (1D-GradAniso-QHA γ): One dimensional gradient anisotropic QHA with the Grüneisen Parameter (1D-GradAniso-QHA γ) uses the same local-gradient approach as 1D-GradAniso-QHA with the addition of the Grüneisen parameter to approximate the vibrational spectra of all expanded structures.

Simulation Details

All calculations were performed using our Python based lattice dynamics code available on GitHub at http://github.com/shirtsgroup/Lattice_dynamics. The code is currently built to run for a test systems and the Tinker 8.1 molecular modeling package⁴⁶ for vibrational spectra, lattice minimizations, and potential energy calculations. The code is designed modularly to be adapted to any program that performs energy minimizations, potential energy and vibrational outputs; we are in the process of incorporating Quantum ESPRESSO.⁴⁷

Lattice structures were retrieved from the Cambridge Crystallographic Data Center with Tinker’s `xtalmin` executable to an RMS gradient/atom of 10^{-5} . When the crystals are expanded, the center of mass for each molecule is moved, preserving the intramolecular distances. The expanded structures are geometry optimized using Tinker’s `minimize` executable with an RMS gradient/atom of 10^{-4} to geometry optimize the crystal. Discussion of minimization criterion can be found in the Supporting Information. In some cases Tinker aborted before this point; both cases for Tinker aborting and choice of RMS is discussed further in the Supporting Information (Section 6).

For each crystal structure, the lattice energy (U) is computed with Tinker’s `analyze` executable. In the cases where the mass-weighted Hessian is calculated, we compute the vibrational spectra using Tinker’s `vibrate` executable. We have edited Tinker’s code to perform a finite difference calculation to compute the second derivative of the charge potential energy function. Discussion of our code adjustments can be found in the Supporting Information (Section 13).

The isotropic Grüneisen parameters were found by solving eq. 9 using the `vibrate` executable on the lattice minimum structure and the lattice minimum structure expanded by $\Delta V/V = 1.5 \times 10^{-3}$. The vibrational spectra of all other isotropically expanded structures were found using eq. 10. The anisotropic Grüneisen parameters were found by solving eq. 9 in all six of the strain directions. For each strain, the crystal matrix parameter (η_i ; $i = 1, 2, \dots, 6$) is increased by $\eta_i = 1.5 \times 10^{-3}$ and using the `vibrate` executable the vibrational spectra of the lattice minimum structure and 6 strained structures are calculated. The vibrational spectra of all other strained structures are found using eq. 14. We also assure that the vibrational modes match correctly between differing volumes, further information can be found in the Supporting Information (Section 15).

Determining the correct numerical step size for computing the gradient of thermal expansion is the main factor in assuring that the crystal remains at a Gibbs free energy minimum up to the temperature of interest. When computing the thermal gradient ($\frac{\partial y}{\partial T}$ where $y = V$, λ , or C_i) there is some finite step size ($\pm \Delta y$) that is required to solve the thermal gradient numerically. We found that the best way to determine Δy for each crystal and method was to pick a step size that would change the lattice minimum energy by 5×10^{-4} kcal/mol. Further discussion of this and a table of the values can be found in the Supporting Information (Section 9).

4 Results and Discussion

4.1 Converging on the Minimum Gibbs Free Energy Structure

The quasi-harmonic approximation computes the Gibbs free energy at a given temperature by minimizing y in the function $f(y, T)$. In this approach, y can be the isotropic volume (V), the crystal lattice tensor (\mathbf{C}), or the scalar λ used in our 1D-anisotropic approach. With the gradient approach, we can easily determine if the structure that is computed to min-

imize f is at a local minimum by estimating if $\frac{\partial G}{\partial y} = G' = 0$. Our code provides an approximate check of whether a point is nearly at the minimum by comparing the backwards, central, and forward finite solutions of $\frac{\partial G}{\partial y}$. Since the first-order errors in $G'_{backwards}$ and $G'_{forwards}$ should be equal and opposite, if the ordering $G'_{backwards} < G'_{central} < G'_{forwards}$ is satisfied then at least at that level of error we are at the minimum.

Most of the gradient approaches described above converged to minimum free energy structures within numerical error at every Runge-Kutta step for all four crystal structures. The only methods that failed to do this for some crystal polymorphs were GradIso-QHA, GradAniso-QHA γ , and 1D-GradAniso-QHA for piracetam form III as well as 1D-GradAniso-QHA for resorcinol form α . For GradIso-QHA with piracetam form III and 1D-GradAniso-QHA with resorcinol form α , we were able to achieve our minimization criterion at every step by increasing the number of Runge-Kutta steps up to 300 K. For both of these methods on these systems only, the results in the following sections will be those achieved with four Runge-Kutta steps instead of three. For the other two methods performed on piracetam form III, we found that the crystal structures were re-structuring at $T > 0K$, indicating a failure in the QHA approach.

4.2 Discontinuities in the Free Energy Surface are Problematic for QHA

QHA will fail when there are multiple minima on the free energy surface which can interconvert when lattice expansion occurs. QHA assumes that there is a single minimum that represents the thermodynamic properties at a given temperature and pressure, which becomes problematic when there are multiple minima present. In our previous work with MD simulations, we observed that a number of crystal structures re-minimized to new structures when the crystal was heated.²¹ However, that is not what is generally happening here. Instead, we

have found that in the process of expansion, even relatively small restructuring can lead to a failure of both the structure and free energy to vary continuously, thus violating the assumptions of QHA. We looked at how the potential energy, free energy, and lattice vectors and angles change with temperature to help quantify the existence of a discontinuity found from thermal expansion. For piracetam form III, we took 20 Runge-Kutta steps up to 300 K for 1D-GradAniso-QHA and GradAniso-QHA γ to help pinpoint where the QHA was failing for both methods. The top two graphs in fig. 4 present the percent change in the lattice parameters, $\%h$, for the three lattice vectors (left) and angles (right). For a particular lattice parameter, h_i , the percent change is calculated as:

$$\%h_i(T) = \frac{h_i(T) - h_i(T = 0 \text{ K})}{h_i(T = 0 \text{ K})} \times 100\% \quad (28)$$

The bottom two plots in fig. 4 show the potential energy (U) and the Gibbs free energy deviation from HA ($G_{QHA} - G_{HA}$). Up until 200 K, both methods provide visually indistinguishable and smooth results for the changes in lattice parameters and energy with temperature. Additionally, our methods produce structures at a free energy minimum ($\frac{\partial G}{\partial \lambda} = 0$ or $\frac{\partial G}{\partial \mathbf{C}} = 0$) up to 255 K for 1D-GradAniso-QHA and to 270 K for GradAniso-QHA γ . After these temperatures the computed lattice parameters and energies have rough transitions with temperature and oscillate.

Discontinuities in the free energy surface are most easily visualized by looking at each atoms movement due to thermal expansion as a function of T . In Cartesian coordinates, a particular atom will have a position vector, $v = [x, y, z]$, that we can track with its temperature change by computing $\frac{\partial l}{\partial T}$ by backwards finite difference, which is shown in eq. 29.

$$\frac{\partial l}{\partial T} = \frac{\|v_i - v_{i-1}\|}{T_i - T_{i-1}} \quad (29)$$

The change in $\frac{\partial l}{\partial T}$ as a function of temperature is shown in fig. 5. Each line represents the motion of a different atom.

The sudden oscillation in the lattice parame-

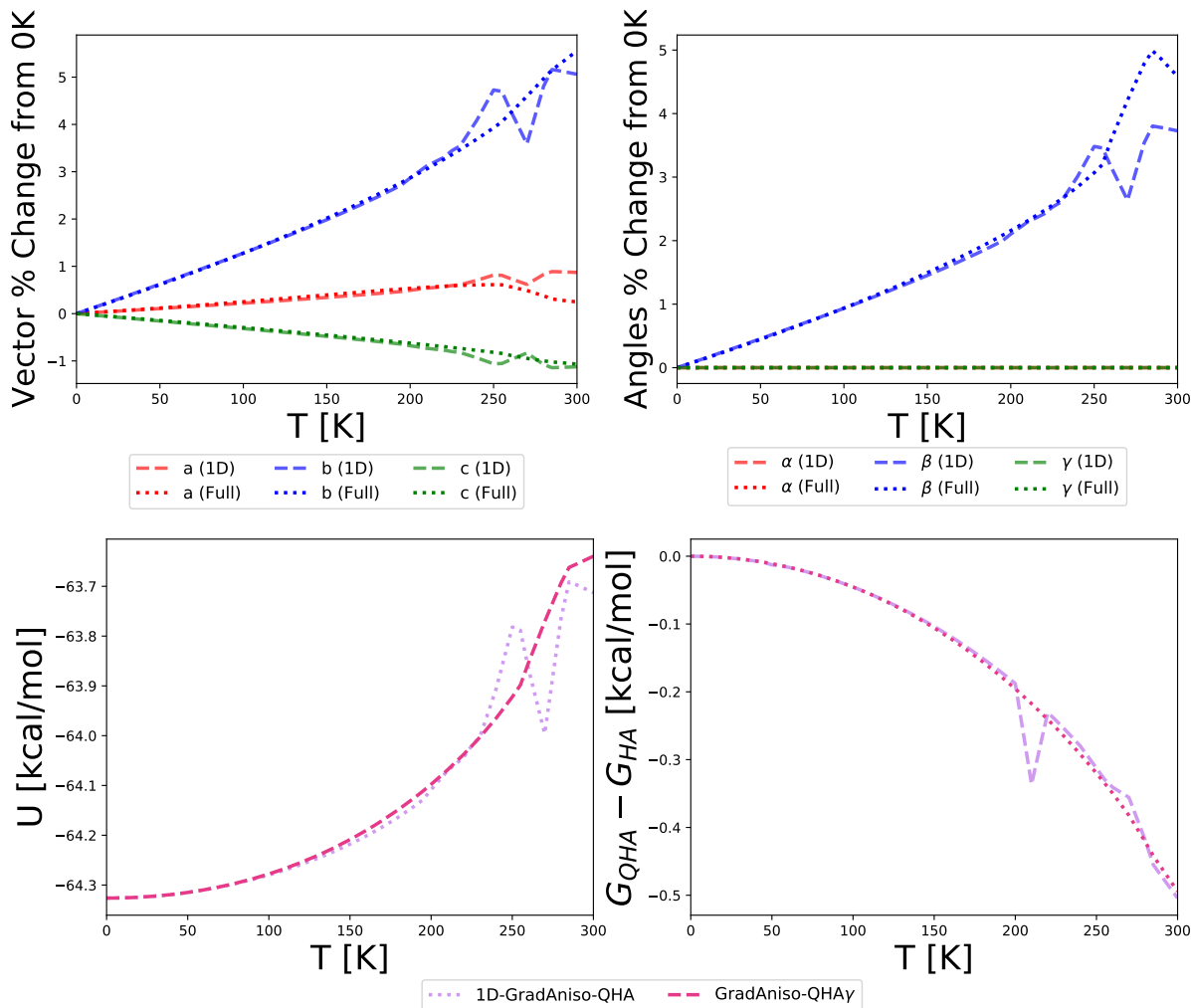


Figure 4: Computed percent change of lattice parameters (top left and right) from 0 K using eq. 28, potential energy U (lower left), and $G_{QHA} - G_{HA}$ (lower right) for piracetam form III using 1D-GradAniso-QHA (1D) and GradAniso-QHA γ (Full). Both methods produce similar, smooth results up to 200 K. After 200 K, the crystal re-structures for both methods, and additionally falls out outside of the free energy minimum as determined by numerical checks of $\partial G/\partial C_i$.

ters and energy are due to adjustments in the molecular arrangement within the crystal. As the crystal expands, new volumes open, which provides new low energy arrangements of individual atoms or entire molecules when geometry optimized. Fig. 5 shows that this behavior is not smooth for some crystals. Up until 200 K 1D-GradAniso-QHA shows that $\frac{\partial l}{\partial T}$ changes smoothly and relatively slowly with temperature (left in fig. 5). After 200 K all of the atoms start to move dramatically faster, leading to the oscillation of lattice parameters and energy at 250 K. Similarly, GradAniso-QHA has a large shift in the coordinates at 250 K (right in fig. 5), which also coincides with roughness

of the curves for the lattice parameters and energy.

For the free energy and lattice expansion of individual polymorphs we compare the results at 300 K, we therefore do not show results for GradAniso-QHA, GradAniso-QHA γ , and 1D-GradAniso-QHA because the system becomes discontinuous before we reach 300 K. Since we show the polymorph free energy differences across the temperature range, we do show GradAniso-QHA γ and 1D-GradAniso-QHA up to 200 K to understand the low temperature behavior.

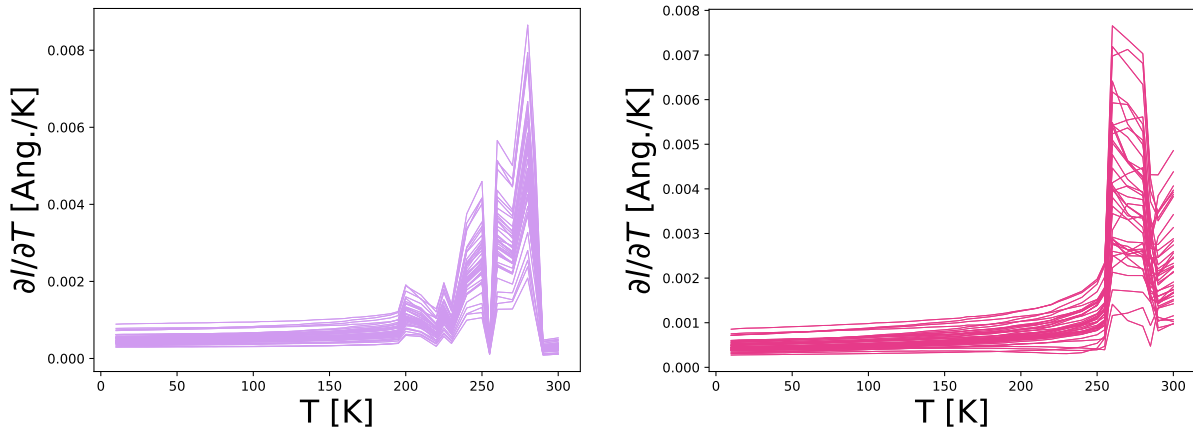


Figure 5: Computed $\frac{\partial l}{\partial T}$ for each atom in the crystal of piracetam form III using 1D-GradAniso-QHA (left) and GradAniso-QHA γ (right) using eq. 29. Each line represents a different atom within the unit cell. Up until that 200 K $\frac{\partial l}{\partial T}$ is smooth, but after 200 K the behavior becomes rough and sharply increases implying a re-structuring of the crystal. We use the same colors for each method that are used in the energy plots of fig. 4.

4.3 Polymorph Gibbs Free Energy

All results for the ten QHA methods are shown as their Gibbs free energy deviation from the harmonic approximation. The results for the full plots of G versus temperature can be found in the Supporting Information (Section 11). Instead, we will summarize the results at 300 K, as shown in fig. 6. As the deviations increase with temperature, the 300 K results represent the largest change.

Our gradient method successfully matches the stepwise approach for isotropic expansion within reasonable numerical error. Although the gradient and stepwise approaches determine the minimum Gibbs free energy volume in different ways, both methods should produce similar results as they solve the same equation. For all four crystal structures the deviations between the stepwise and gradient approach are less than 0.0002 kcal/mol at 300 K, which is smaller than the required energy tolerances in literature for organic polymorphs.

The Grüneisen approaches have small, but noticeable effects on the predicted Gibbs free energy for isotropic expansion. For all four crystals, there is less than a 0.04 kcal/mol deviation between all isotropic methods. This deviation

is largest, 0.039 kcal/mol, for piracetam form I when comparing the computed free energy at 300 K for GradIso-QHA and GradIso-QHA γ . For all other crystals, the difference between Grüneisen and non-Grüneisen approaches is < 0.013 kcal/mol.

By removing constraints on the crystal lattice parameters and thus increasing the accuracy of the thermal expansion we find that the crystal is able to expand into a lower Gibbs free energy minimum for all crystals, as would be anticipated as constraints are removed from a minimization. As a validation, the following ranking of free energy for methods should hold true for all T .

$$G_{HA} > G_{Isotropic-QHA} \geq G_{Anisotropic-QHA} \quad (30)$$

We see that the free energies in fig. 6 indeed satisfy this condition for all crystals.

For resorcinol, our three anisotropic methods converge to the same result within error, but the Grüneisen approaches overestimate the decrease in free energy due to anisotropic thermal expansion. For the three different anisotropic methods there is a difference in the computed free energy that is less than 0.002 kcal/mol at 300 K. In the top graph of fig 6 the only visible differences between the 6 anisotropic

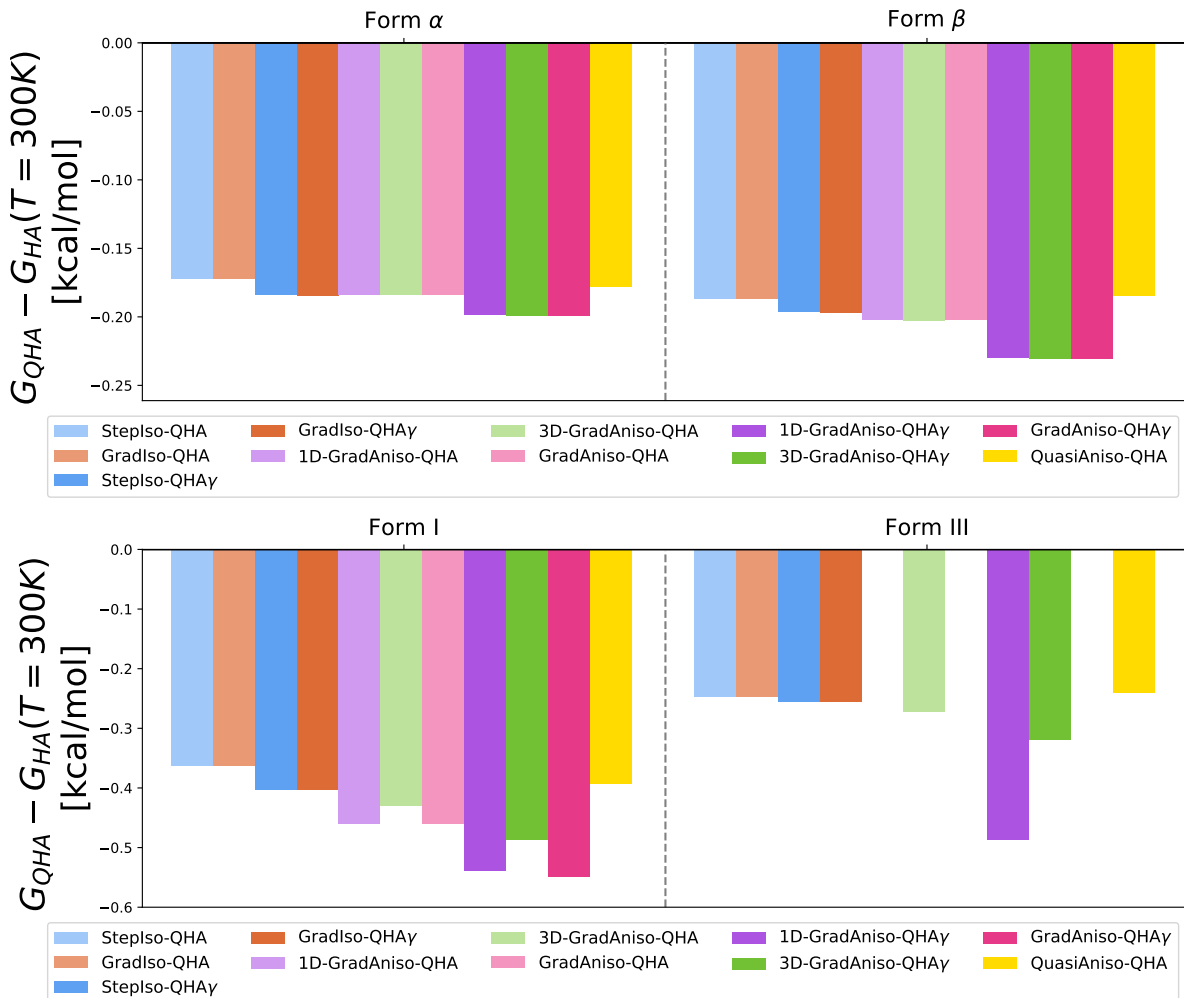


Figure 6: The Gibbs free energy deviations of the QHA methods from HA which completed are shown at 300 K for resorcinol (top) and piracetam (bottom). By removing constraints from the thermal expansion model, the crystal relax into a lower free energy structure. The largest differences in free energy for the 10 QHA methods are due to using the Grüneisen parameter. The results for 1D-GradAniso-QHA γ , GradAniso-QHA, and GradAniso-QHA γ for piracetam form III are not shown because of discontinuities in the free energy as a function of T , as discussed in section 4.2.

methods are between the three with full Hessian calculations and the Grüneisen approaches (i.e. comparing 1D-GradAniso-QHA with 1D-GradAniso-QHA γ , 3D-GradAniso-QHA with 3D-GradAniso-QHA γ , and GradAniso-QHA with GradAniso-QHA γ), all of which are < 0.03 kcal/mol.

Piracetam has greater variability between our six anisotropic QHA methods, even among those that do not use the Grüneisen parameter approximation. In the bottom graph of fig. 6 the results for 1D-GradAniso-, GradAniso-QHA, and GradAniso-QHA γ are not shown for form III because of the discontinuities discussed

in section 4.2. The 1D-, 3D-, and unconstrained anisotropic thermal expansion methods deviate by 0.03–0.17 kcal/mol. The main reason is the fact that the off-diagonals in the lattice tensor change as temperature increases, which is not captured in the 3D expansion approach. Methods using the Grüneisen approach differ from those using the full Hessian calculations by between 0.05–0.09 kcal/mol.

Ignoring thermal expansion is inappropriate for these crystal structures, but the difference between isotropic and anisotropic methods is crystal dependent. Overall, thermal expansion can reduce the free energy computed in the

harmonic approximation by 0.17–0.46 kcal/mol for methods that compute the full Hessian or 0.18–0.55 kcal/mol for Grüneisen approaches. Isotropic expansion makes up the majority of this difference, up to 0.36 and 0.40 kcal/mol for full Hessian and Grüneisen approaches, respectively. The anisotropic methods only reduce the free energy by 0.01–0.04 kcal/mol for resorcinol and 0.02–0.23 kcal/mol for piracetam. The largest deviation between isotropic and anisotropic approaches comes from piracetam form III where 1D-GradAniso-QHA γ is 0.23 kcal/mol lower in energy than the isotropic Grüneisen approaches.

QuasiAniso-QHA converges to high temperature free energies more similar to isotropic expansion rather than anisotropic expansion. The quasi-expansion approach deviates between 0.02–0.23 kcal/mol from all fully anisotropic methods. For piracetam form III and resorcinol form β the 300 K free energy computed by QuasiAniso-QHA is actually higher than GradIso-QHA. The lattice energy, $U(V)$, is always lower in energy for Quasi-Aniso-QHA than the isotropic methods (as it must be). However, we found that the vibrational contribution to the free energy made the quasi-anisotropic structure less favorable at higher temperatures, leading to minimization at different structural points. The quasi-anisotropic approach ranged between -0.006–0.03 kcal/mol of GradIso-QHA at 300 K, frequently being higher in free energy than GradIso-QHA at these temperatures, as compared to lower free energy, more accurate 1D-GradAniso-QHA and GradAniso-QHA methods (and their Grünisen variants). Further detail and analysis can be found in the Supporting Information (Section 12).

4.4 Gibbs Free Energy Differences of Polymorphs

The Gibbs free energies of individual polymorphs are not physically relevant; the physically relevant observable that determines their stability is the Gibbs free energy difference between the polymorphs. It is often assumed that errors in the type of thermal expansion,

finite size effects, anharmonic motions, and Grüneisen parameter, and even to some extent the potential energy function used to model the crystal structure can be neglected because of cancellation effects in polymorph free energy differences.

We therefore desire to determine if errors in the type of thermal expansion and the use of the Grüneisen parameter cancel for polymorph free energy differences. In fig. 7 the deviations of polymorph free energy differences for QHA are shown from HA. We quantify the deviations ($\Delta\Delta G_{i,j}$) by eq. 31, where $\Delta G^{i,j}$ is the free energy difference between polymorphs i and j .

$$\Delta\Delta G_{i,j} = \Delta G_{QHA}^{i,j} - \Delta G_{HA}^{i,j} \quad (31)$$

Comparing the polymorph free energy differences, we see that all QHA methods compute $\Delta G_{i,j}$ within 0.02 kcal/mol or 0.12 kcal/mol from each other for resorcinol and piracetam respectively. Since there is such negligible difference between stepwise and gradient isotropic approaches, the results for StepIso-QHA and StepIso-QHA γ are not shown. The isotropic Grüneisen approaches have the largest deviations from other isotropic methods. The largest deviation due to use of the Grüneisen approaches is 0.0025 kcal/mol for resorcinol and 0.025 kcal/mol for piracetam at 300 K.

Anisotropic expansion yields little change to the polymorph free energy differences for resorcinol, but provides a greater difference for piracetam, as shown in fig. 7. For resorcinol, the polymorph free energy difference between isotropic approaches and unconstrained anisotropic expansion increases with temperature, but the overall deviation of 0.02 kcal/mol is relatively small. In contrast, the type of thermal expansion can significantly alter the final free energy difference for piracetam. Despite the re-structuring in piracetam form III we are able to show the results for GradAniso-QHA γ up to 200K, prior to failure. At temperatures less than 200 K, we see that 1D-GradAniso-QHA γ is nearly indistinguishable from GradAniso-QHA γ , implying that the 1D approach is a more accurate model for anisotropic thermal expansion than the 3D ap-

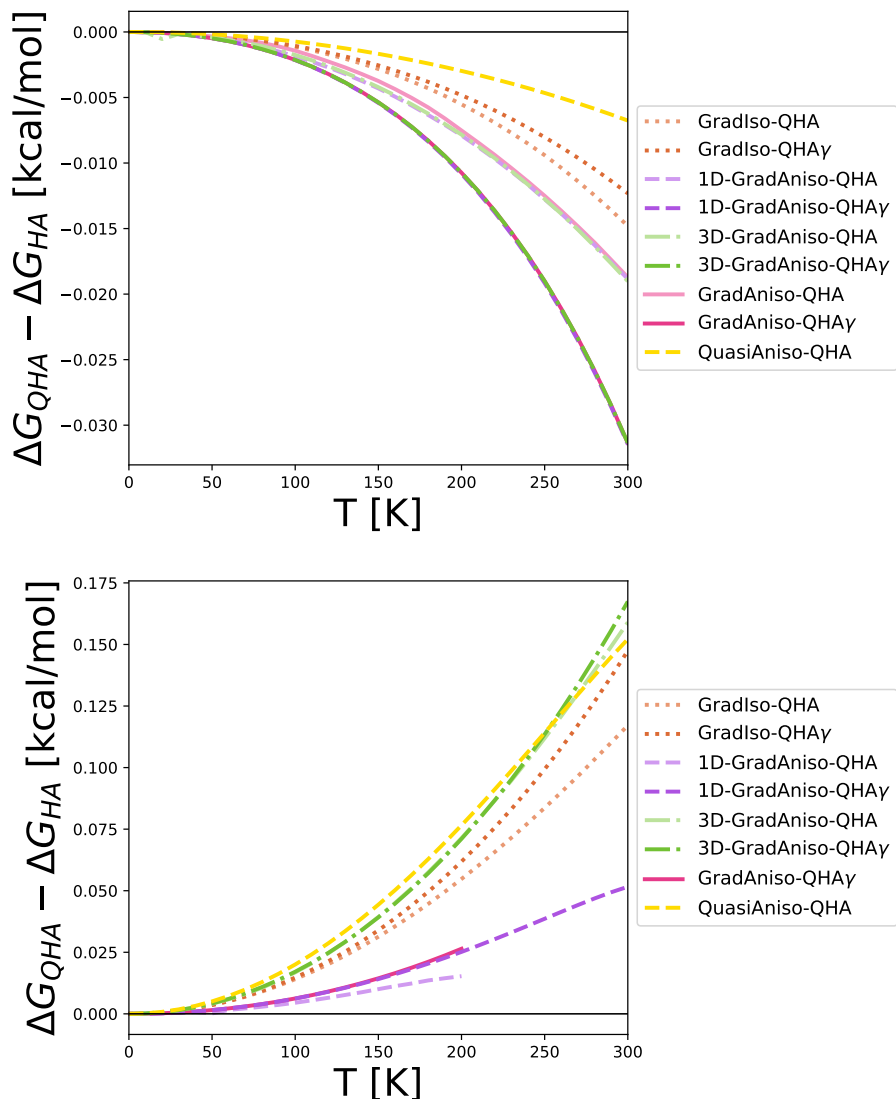


Figure 7: Computed polymorph Gibbs free energies differences for the QHA methods shown as their deviation from the harmonic approximation using eq. 31 for resorcinol (top) and piracetam (bottom). The top graph shows that all QHA methods predict the free energy differences within 0.02 kcal/mol of each other for resorcinol. The bottom graph shows that all QHA methods predict the free energy differences with 0.12 kcal/mol for piracetam. Plots for 1D-GradAniso-QHA and GradAniso-QHA γ are truncated and GradAniso-QHA omitted in piracetam because of lower temperature problems with restructuring on expansion (see Section 4.2).

proach. In particular, changes in the off-diagonal elements of the crystal tensor are responsible for a 0.08–0.12 kcal/mol change in $\Delta G_{i,j}$ from all other methods at 300 K for 1D-GradAniso-QHA γ and the other methods.

The quasi-anisotropic QHA method computes the free energy differences of the polymorphs only to within 0.025–0.1 kcal/mol of our most accurate method for the molecules tested, as

shown in fig. 7. For resorcinol, the quasi-anisotropic approach performs slightly worse than the isotropic methods relative to the GradAniso-QHA and GradAniso-QHA γ , but the energy gaps between all methods are less than 0.025 kcal/mol. For piracetam, the agreement between GradAniso-QHA γ and 1D-GradAniso-QHA γ at low temperatures strongly suggests that at 300 K, 1D-GradAniso-QHA γ

is the most accurate method, and QuasiAniso-QHA deviates by 0.1 kcal/mol from this approach at that temperature.

4.5 Lattice Expansion

Changes in the Gibbs free energy and free energy differences between different QHA approaches are due to the varying lattice geometries at high temperatures. We evaluate those changes by computing the percent change in the lattice vectors and angles (eq. 28) for all four crystals. We compare the percent lattice change at 300 K, $\%h(T = 300 K)$, where the percent expansion will be greatest.

The results for all eight gradient QHA methods in fig. 8 show the distinct differences for how the crystals expand for isotropic and anisotropic thermal expansion. Stepwise approaches are not shown because they are within numerical error of the gradient approach. For each radar plot, the left shows the percent change in the vectors and the right shows the percent change for the lattice angles. All percent changes are from 0 to 300 K as computed with eq. 28. If the points of the triangle lie within the white region there is a percent increase and the gray region signifies a percent decrease of the parameter. All isotropic methods have the same percent change in the lattice vectors and no change in the angles. All isotropic methods converge to the same lattice geometry at $T > 300$ K within numerical error, as expected. The isotropic methods are plotted as the solid lines on the radar plots. Close examination of the four isotropic QHA methods shows that the predicted expansion of lattice parameters are visually indistinguishable across all four methods. The largest range of the percent expansion of lattice vectors is 0.19% and that is for piracetam form I, which is small relative to the differences due to anisotropic expansion. Despite the errors in the Gibbs free energy when using the Grüneisen approaches, all four methods converge to the same minimum energy lattice geometry.

Isotropic expansion largely underestimates the changes in the lattice vectors due to thermal expansion, and also misses important changes

in the angles. For all four crystals, we can see that the triangles on the radar plots for the lattice vectors represent a completely different set of percent expansions from the isotropic methods. In all four crystals we see that one vectors expands about 2–4% more than the isotropic methods. Alternatively, we can see that only one angle changes for both polymorphs of piracetam, but that percent expansion can be as large as a 4% change in the angle, which supports the large energy differences seen between the methods.

The quasi-anisotropic approach produces similar high temperature lattice geometries as the anisotropic approaches for resorcinol, but not piracetam. For both crystal structures of resorcinol, the results with the quasi-anisotropic approach are somewhat different from the fully anisotropic methods, but do qualitatively capture the same expansion trends. This is contrasted with piracetam, where the quasi-anisotropic approach produces a high temperature lattice geometry that is much closer to isotropic expansion than to the anisotropic expansion. These results are only for a small data set, and thus may not be representative of results obtained with other molecules.

4.6 Success of One-Dimensional Anisotropic Gradient QHA

Our one-dimensional anisotropic gradient approach produces results similar to the unconstrained anisotropic gradient method and is only slightly more computationally expensive than the gradient isotropic approach. For the free energy, free energy differences, and lattice expansions we see that 1D-GradAniso-QHA and 1D-GradAniso-QHA γ are indistinguishable from GradAniso-QHA and GradAniso-QHA γ , respectively. Additionally, the discontinuity found in the unconstrained anisotropic expansion of piracetam form III is also found by 1D-GradAniso-QHA. While these results are for only two pairs of polymorphs, the accuracy thus far is promising especially considering the speed of 1D-GradAniso-QHA. In table 2 the number of geometry and optimizations for each method are provided. We can see that

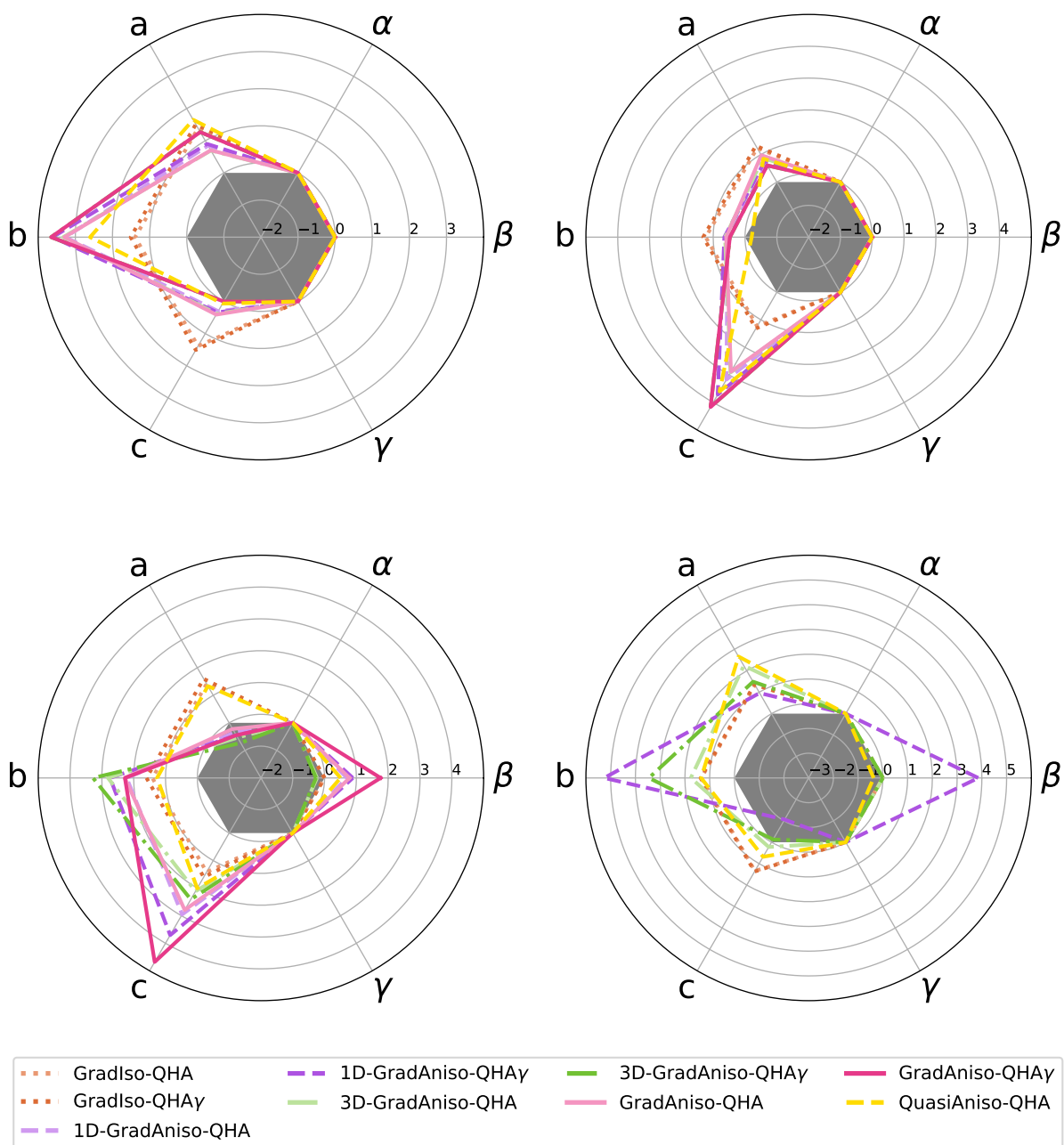


Figure 8: Computed percent change of lattice parameters from 0 to 300 K for resorcinol form α (top left) and β (top right), as well as piracetam form I (bottom left) and III (bottom right). The white region reflects a percent increase with temperature, while the gray region is a percent decrease. The change in the lattice parameters show distinct differences between isotropic and anisotropic expansion.

our one-dimensional approach will be slightly slower than the isotropic method, but requires much less computational time compared to the unconstrained approach.

5 Conclusions

We have presented a novel method for calculating both isotropic and anisotropic expansion of crystalline materials in the quasi-harmonic approximation. We compare our new gradi-

Table 2: For a select number of methods we show how many geometry optimizations and Hessian calculations are required. We provide a range for the anisotropic methods because specific pieces of the lattice tensor may be zero, in which case the gradient at those points are not calculated. All of these results are for the we laid out previously in our methods section.

Number of Sub-Routines		
Method	Number of Geometry Optimizations	Number of Hessians
GradIso-QHA	39	39
1D-GradAniso-QHA	58–112	58–112
GradAnsio-QHA	247–949	247–949
GradIso-QHA γ	39	3
1D-GradAniso-QHA γ	64–118	7
GradAnsio-QHA γ	253–955	7

ent approach to established stepwise grid search methods for isotropic thermal expansion as well as quasi-anisotropic approaches and find that the stepwise and gradient approaches are essentially indistinguishable. Additionally, we demonstrate that our approach is easily extended to more complex anisotropic expansion and show how we can limit the degree of anisotropy sampled with the method.

Our gradient method produces results within numerical error of the isotropic stepwise approach, but we do note that assuming the Grüneisen parameter is constant can lead to non-negligible deviations in the free energy at high temperatures. The computed free energy at 300 K for stepwise and gradient isotropic approaches are within 0.0002 kcal/mol for all crystals. However, Grüneisen approximation approaches can vary up to 0.04 kcal/mol at 300 K from methods that compute the full Hessian. Some of the error caused by the Grüneisen approximation is canceled when looking at polymorph free energy differences. All four isotropic QHA methods compute the 300 K polymorph free energy differences within 0.025 kcal/mol for both resorcinol and piracetam.

For these crystals, high temperature lattice geometries differ significantly with anisotropic expansion versus isotropic expansion, but not for quasi-anisotropic QHA. For isotropic expansion, the lattice vectors have equal percent expansions (1–2%) from 0 to 300 K and the lattice angles remain fixed. For anisotropic expansion the lattice vectors change between -1–5% and both crystals of piracetam exhibited a change

in the β angle. Quasi-anisotropic QHA matches our anisotropic approaches to within 0.5% expansion of each lattice parameter for resorcinol, but misses the anisotropic nature of the crystals of piracetam and closely resembles the isotropic expansion trends.

The effect of adding anisotropic expansion on the free energies is system dependent, but even for cases where it is important there is a cancellation of error in the free energy differences between polymorphs. Anisotropic expansion reduces the crystal free energy at 300 K by 0.01–0.23 kcal/mol relative to isotropic expansion because of the removal of the isotropic constraints. However, these changes in free energy resulted in changes in the free energy differences between polymorphs of only 0.01–0.12 kcal/mol compared to isotropic expansion, showing that a large amount of the error in the isotropic model is canceled in the relative energy differences between polymorphs. Anisotropic expansion is more important for piracetam than for resorcinol, with differences in free energy and free energy differences between polymorphs using anisotropic versus isotropic expansion for piracetam approximately twice those for resorcinol.

Our thermal gradient approach demonstrates that minimization of the full free energy, and not just the lattice energy, is important when treating anisotropic expansion effects on high temperature lattice geometry and free energy. Including anharmonic effects fully is less relevant for polymorph free energy differences, however. Despite the fact that the free ener-

gies of the crystals at 300 K can differ by 0.02–0.23 kcal/mol quasi-anisotropic and anisotropic approaches, the free energy differences are all within 0.025 kcal/mol. Overall, the quasi-anisotropic approach provides somewhat better insight into the crystal properties relative to isotropic expansion, but is problematic in at least some molecules. The introduction of our gradient approach allows us to perform a full free energy minimization of the crystal lattice with similar efficiency, at least in the case the 1D variant.

A significant challenge when utilizing any lattice dynamic method is to assure that the method is sampling only one free energy minimum across the entire temperature range of interest. As we saw with piracetam, two anisotropic QHA methods failed due to a restructuring of the crystal upon expansion to higher than 200 K, a scenario which QHA is not designed to handle for more complex crystals where almost certainly multiple minima are accessible. Issues like this are likely to become more problematic with more complex molecules and increased number of variables in the optimization, as with 1D-GradAniso-QHA and GradAniso-QHA γ . Our best recommendation for identifying potential failures is to take more Runge-Kutta steps until $\frac{\partial G}{\partial y} = 0$ ($y = V, \lambda, C_i$) or $\frac{\partial l}{\partial T}$ quickly increases / oscillates, indicating some sort of structural discontinuity in the expansion.

For the model systems presented in this paper, we have successfully shown that our gradient approach provides a reasonably fast way to perform QHA with an fully anisotropic thermal expansion model. In these test systems, we saw that the lattice parameters relaxed anisotropically because of the availability of lower free energy geometries. While the number of molecules studied here is small, it demonstrates the viability of the approach presented here and shows that further exploration of the effects of anisotropic expansion is necessary.

Acknowledgments

The authors thank Eric Dybeck and Natalie Schieber for help with discussion regarding of the importance of anisotropic thermal expansion and practicality of implementing the gradient method. We also thank Graeme Day, Gregory Beran, and Aaron Holder for input of the manuscript prior to submission. Testing and development of our methods / code as well final results were performed on the Extreme Science and Engineering Discovery Environment (XSEDE), which is supported by National Science Foundation grant number ACI-1548562. Specifically, it used the Bridges system, which is supported by NSF award number ACI-1445606, at the Pittsburgh Supercomputing Center (PSC). Testing was also performed on Summit super computer, which is supported by the NSF grant OAC-1532235. This work was supported financially by NSF through the grant nsf-cbet 1351635.

Supporting Information for “A Thermal Gradient Approach for the Quasi-Harmonic Approximation and its Application to Improved Treatment of Anisotropic Expansion”

All results shown here and in the main text are for the symmetric unit cells. We present how we chose the various parameters required in the paper. These include:

1. Standard error of Tinker’s vibrational frequencies
2. Dependence of the Grüneisen parameter on finite difference step size
3. Stepwise isotropic QHA grid spacing
4. Gradient finite difference step size for isotropic, anisotropic, and 1D-anisotropic expansion
5. Comparison of Euler and Runge-Kutta step sizes
6. Full polymorph free energies summarized in the paper
7. Analysis of quasi-anisotropic lattice energies and free energies
8. Modifications required for Tinker
9. Details of calculation of the Grüneisen parameter using the strain
10. Matching vibrational modes
11. Description of the constrained volume optimization procedure

We also show the polymorph free energy differences for each crystal up to 300 K, modifications we had to make to Tinker, and discussion of how we computed the strain tensor for the Grüneisen parameter. All unit cells were retrieved from Cambridge Crystallographic Data Center. The corresponding reference codes are BISMEV03 for piracetam form I, BISMEV02 for piracetam form III, RESORA03 for resorcinol form α and RESORA08 for form β .

6 Standard Error of Tinker’s Vibrational Frequencies

Obtaining a highly accurate crystal vibrational spectra is both one of the most important and hardest parts of converging on a numerically stable QHA result. We determine the sensitivity of the vibrational spectra from Tinker’s `vibrate` executable based on the tolerance used in the geometry optimization, `minimize`, for the crystals studied. Aspects like the Hessian tolerance and PME-grid spacing effect the vibrational sensitivity, the minimization criteria provides the greatest reduction in error.

We compute the sensitivity by taking the 4 lattice minimum structures and isotropically expanding them by 0.001, 0.002, 0.003, 0.004% V . Each structure was geometry optimized to an RMS gradient per atom tolerance of 10^{-N} , where $N = 2, 3$, and 4 using `minimize` and the vibrational spectra are calculated with `vibrate`. We assume that within the 0.004% V change the individual vibrational modes should be approximately equal to one another another and therefore can be fitted to a linear approximation with a slope of zero. This approximation is different than that made with the Grüneisen parameter since we are working with such small volume changes. We computed the standard error of a linear fit to each vibrational mode versus volume, and report the average of all $3N$ vibrational modes (N is the number of atoms per unit cell). These results can be seen in fig. 9.

In the case of form β resorcinol, the average standard error in the wavenumbers can be reduced by an order of magnitude from $N = 2$ to $N = 4$. Using a geometry optimization of 10^{-4} RMS gradient per atom tolerance sufficiently reduces the standard error and we see little reduction in error between $N = 3$ and 4. We chose a geometry optimization tolerance of 10^{-4} .

Converging the gradient to 10^{-4} in Tinker is numerically difficult and the subroutine occasionally exits without complete convergence. For minimizations that terminate prematurely,

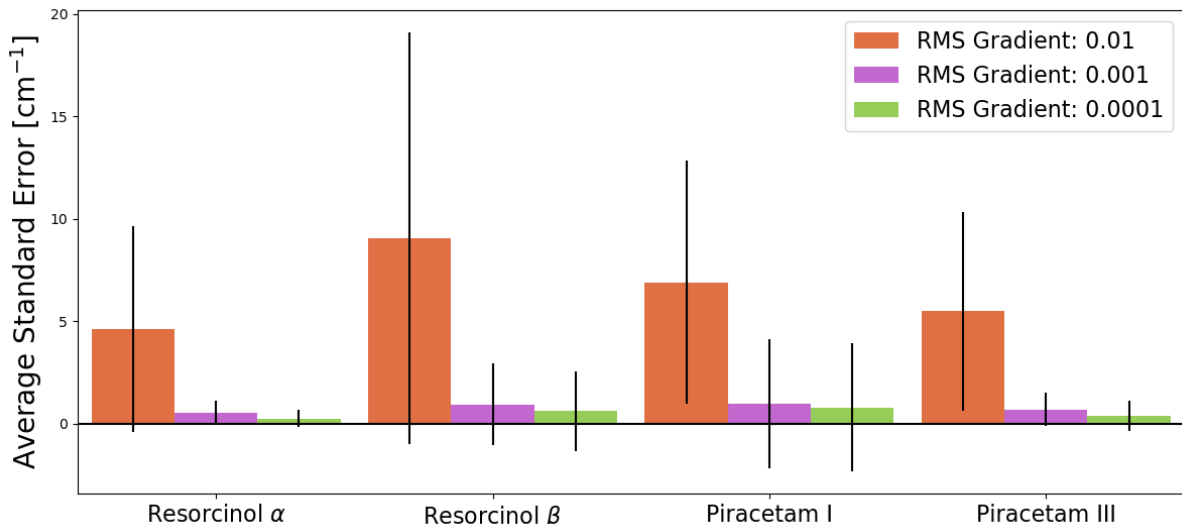


Figure 9: A geometry optimization tolerance of 10^{-4} RMS gradient per atom reduces the sensitivity of the crystal vibrational spectra by an order of magnitude relative to a tolerance of 10^{-2} . Error bars show that individual modes may have larger standard error.

we implemented a subroutine that shifts the atoms Cartesian coordinates in a random direction by less than 10^{-7} Å and attempts to re-minimize the structure. If the minimization does not converge within ten minimizations, the final structure, aborted in the 10^{th} minimization is used as the geometry optimized structure since the energies of all ten structures will be < 0.001 kcal/mol in difference. We found that about 5% of the minimized structures could not reach a tolerance of 10^{-4} within the 10 rounds of our shake algorithm. If the desired tolerance is not reached a warning is output to the user, but the program continues using the structure output from the 10^{th} minimization.

7 Dependence of the Grüneisen Parameter on Finite Difference Step Size

The Grüneisen parameters are solved numerically, so we want to determine how the Grüneisen parameters as we deviate from the lattice minimum structure. For all Grüneisen step sizes, we only ran test for piracetam, but

the same response is expected for resorcinol.

7.1 Isotropic Grüneisen Parameter

As stated in the main paper, the isotropic Grüneisen parameters are solved using a forward finite difference approach. The numerical solution is shown in the following equation:

$$\gamma_k = -\frac{\ln(\omega_k(V + \Delta V)) - \ln(\omega_k(V))}{\ln(1 + \frac{\Delta V}{V})} \quad (32)$$

To solve eq. 32 we need to know the vibrational spectra of our lattice minimum structure and one isotropically expanded structure. To determine the appropriate value of $\Delta V/V$ for that expanded structure, we will look at how the Grüneisen parameters deviate from their value when $\Delta V/V \rightarrow 0$, where QHA is accurate. We plot the values of eq. 33, which is a unitless quantity, for varying $\Delta V/V$ to determine the appropriate step size. From this, we can determine how much the average Grüneisen parameter deviates from the low ΔV limit and look at a confidence interval for the deviations for all

individual modes.

$$\sum_{k=1}^N \frac{\gamma_k - \gamma_{k,0}}{N} \quad (33)$$

N is the total number of vibrational modes, γ_k is the k^{th} modes Grüneisen parameter solved using $\Delta V/V$, and $\gamma_{k,0}$ is the same modes Grüneisen parameter as $\Delta V/V \rightarrow 0$. The value of $\Delta V/V \rightarrow 0$ is actually at $\Delta V/V = 10^{-3}$, any lower value is numerically unstable as determined by the standard error in the angular frequencies.

The results in fig. 10 show the change in the Grüneisen parameter as we deviate from $\Delta V/V = 10^{-3}$ is small as shown by the green line, but that is not the case for individual modes. The 95% confidence interval shown in red shows that the individual Grüneisen parameters can deviate up to 0.5 (unitless) from the Grüneisen parameters for $\Delta V/V = 0$, which can be significant for the majority of Grüneisen parameters that are localized around zero. For small step sizes, $\Delta V/V < 10^{-3}$, the solution for the Grüneisen parameter is numerically unstable because of the standard error in Tinker’s vibrational spectra. A step size of $\Delta V/V = 1.5 \times 10^{-3}$ is a small enough step size to reduce deviations of the Grüneisen parameters from our limit and also assures us that numerical instabilities due to small step sizes are avoided.

7.2 Anisotropic Grüneisen Parameter

The anisotropic Grüneisen parameter is also solved using a forward finite difference approach for the six different strains (3 normal and 3 shear strains), seen in eq. 34.

$$\gamma_{k,i} = -\frac{\ln(\omega_k(\eta_i)) - \ln(\omega_{k,0})}{\eta_i} \quad (34)$$

We will use a similar formalism as the isotropic case to look at deviation in the Grüneisen parameters:

$$\sum_{k=1}^N \frac{\gamma_{k,\eta_i} - \gamma_{k,\eta_i,0}}{N} \quad (35)$$

Where γ_{k,η_i} is the Grüneisen parameter for mode k due to strain η_i and $\gamma_{k,\eta_i,0}$ is the parameter solved for $\eta \rightarrow 0$.

Figure 11 shows the results for both crystals and deviations of the 6 strain Grüneisen parameters. Once again, the average deviation is close to zero, but the highlighted 95% confidence interval is an order of magnitude larger than the deviations in the isotropic Grüneisen parameters. While anisotropic parameters are larger than the isotropic parameters, they are not an order of magnitude larger. This highlights the need to use a small step size for η_i in eq. 34, which is why we will use a step size of $\eta_i = 2.5 \times 10^{-3}$.

8 Stepwise Isotropic QHA Grid Spacing

To assure that the stepwise methods are converging onto correct structure minimizing the free energy, we want to assure that there is sufficiently fine sampling in the volume between the maximum expanded and compressed structures. To do this, we have run StepIso-QHA γ with varying values of $\Delta V/V$ and compare the convergence of $G(T = 300K)$ and smoothness of $V(T)$. The effects of sampling points will effect both StepIso-QHA and StepIso-QHA γ in the same manner, so we use StepIso-QHA γ to reduce the computational expense.

In Figure 12 the results for both crystals of piracetam are reported. The left y-axis reports the $G(T = 300K)$, the right y-axis reports the residuals of a second order fit to $V(T)$, and the x-axis has varying values of $\Delta V/V$ for StepIso-QHA γ . For all step sizes chosen we see that there are little deviations in $G(T = 300K)$, the largest deviation is for piracetam form II with a deviation from the minimum energy (teal line) of 0.002 kcal/mol. The largest influence on the step size is the smoothness of the fit to $V(T)$, which becomes larger with the value of $\Delta V/V$. Based off of these figures, we have decided that $\Delta V/V = 10^{-3}$ is sufficient to converge onto the true isotropic QHA minimum for both stepwise methods.

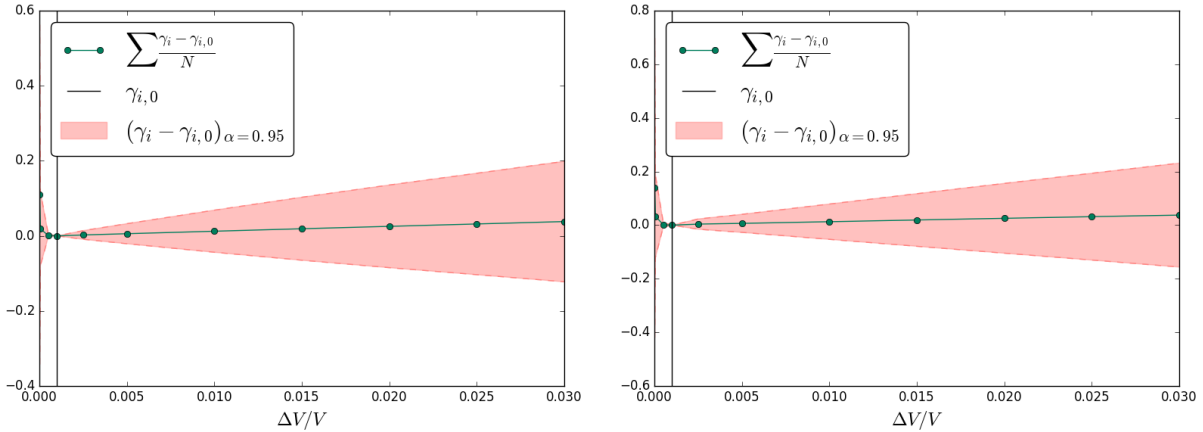


Figure 10: Deviations in the isotropic Grüneisen parameters for piracetam polymorph I (left) and III (right). The line is the average change in all of the parameters and the shaded region is the 95% confidence interval of all individual modes. Small step sizes produces unstable results and large step sizes does not affect the average deviations, but can greatly impact individual modes.

9 Gradient Finite Difference Step Size

As stated in the main paper, the best method for determining the finite step size for computing any of the gradients is to pick a step size that increased the potential energy of the lattice minimum structure by 0.0005 kcal/mol. This cut-off will change depending on the numerical accuracy of the program used to compute the wavenumbers and potential energy, and to perform minimizations. In our program, the user can input some value f or the program can determine the best value of f , where f is defined as:

$$f = \frac{\Delta y}{y_0} \quad (36)$$

Where y can be V or C_i ; y_0 is the value of y at the lattice minimum structure; and Δy is the finite step size used to solve the thermal gradient ($\frac{\partial y}{\partial T}$). Further context of Δy is in the following sections.

For each method (isotropic, anisotropic, and 1D-anisotropic) we perform an initial search for a value of Δy where $\Delta U > 0.0005$ kcal/mol. Here, ΔU is:

$$\Delta U = U(y_0 + \Delta y) - U(y_0) \quad (37)$$

We do this for values of $f = 10^{-N}$ and 5×10^{-N} for values of $N = 5, 4, 3, 2$, and 1. We use the first value of Δy that exceeds our cut-off for Tinker and that value for Δy is used to compute every gradient in the run.

9.1 Isotropic QHA

As stated in the main paper, we have used a finite difference approach to solve eq. 38.

$$\frac{\partial V}{\partial T} = \frac{\left(\frac{\partial S}{\partial V}\right)}{\left(\frac{\partial^2 G}{\partial V^2}\right)} \quad (38)$$

Where the numerator and denominator are solved with a central finite difference approach:

$$\frac{\partial S}{\partial V} = \frac{S(V + \Delta V) - S(V - \Delta V)}{2\Delta V} \quad (39)$$

$$\frac{\partial^2 G}{\partial V^2} = \frac{G(V + \Delta V) - 2G(V) + G(V - \Delta V)}{(\Delta V)^2} \quad (40)$$

Fig. 13 shows the results for piracetam form I for how ΔU changes as a function of f . We can see that the first step to exceed our cut-off is $f = 5 \times 10^{-3}$. Therefore, we will ΔV for all gradients will be set to $V_0 \times 5 \times 10^{-3}$. For all four crystals the value of f was set to 5×10^{-3} .

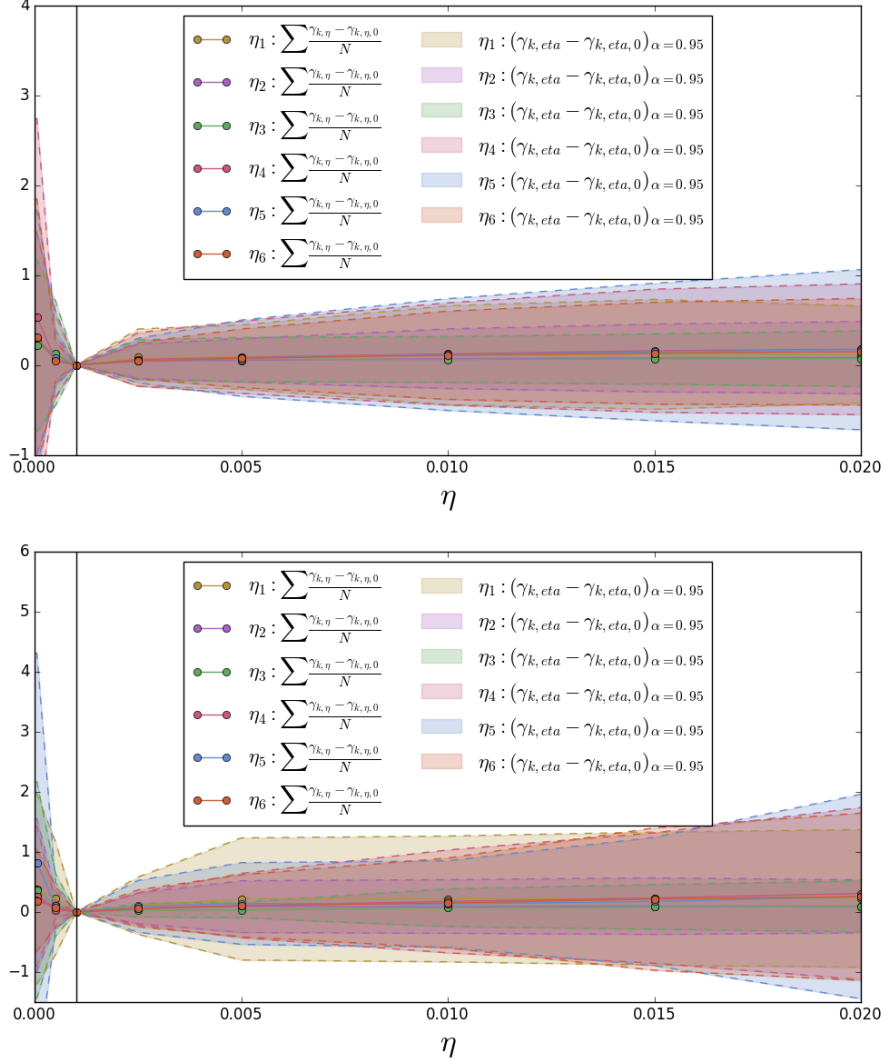


Figure 11: Deviations in the anisotropic Grüneisen parameters for piracetam polymorph I (top) and II (bottom). The lines are the average change in all of the parameters and the shaded region is the 95% confidence interval of all individual modes. The anisotropic Grüneisen parameters deviate by an order of magnitude due to the step size in comparison to the isotropic case. Using a small step size is very important to model the free energy accurately at low temperatures.

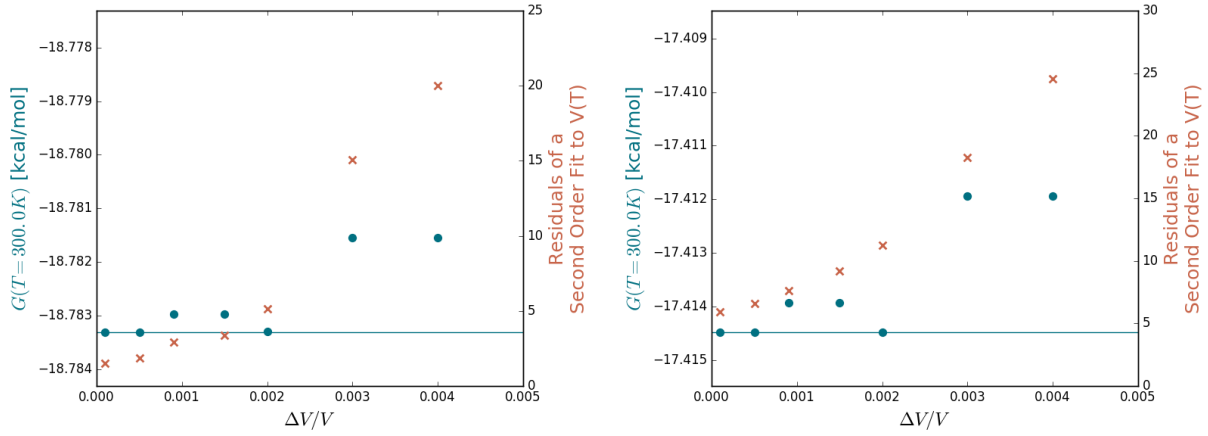


Figure 12: Step sizes between adjacent isotropically expanded structures for stepwise isotropic QHA to show the convergence of $G(T)$ and smoothness of $V(T)$ for piracetam polymorph I (left) and III (right). The step sizes chosen here, have little influence on the free energy convergence at 300K, but have a large influence on the smoothness of $V(T)$. The teal line is the minimum Gibbs free energy computed for all step sizes.

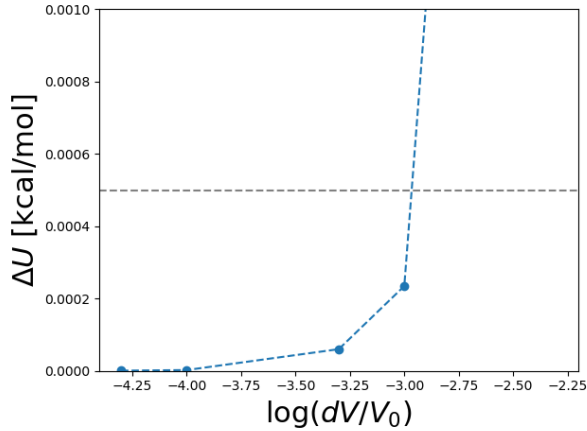


Figure 13: Changes in the potential energy of the lattice minimum structure of piracetam form I, when changing the isotropic volume by varying values of $f = \Delta V/V_0$. The energy exceeds the required cut-off when $f = 5 \times 10^{-3}$.

9.2 Anisotropic QHA

We also solved for the anisotropic gradients, eq. 41, with a finite difference approach.

$$\frac{\partial \mathbf{C}}{\partial T} = \left(\frac{\partial^2 G}{\partial \mathbf{C}^2} \right)^{-1} \frac{\partial S}{\partial \mathbf{C}} \quad (41)$$

The second derivative of the free energy with the strain is a 6×6 matrix, where the diagonals are solved for C_i as:

$$\frac{\partial^2 G}{\partial C_i^2} = \frac{1}{\Delta C_i^2} (G(T, \mathbf{C} + \Delta C_i) - 2G(T, \mathbf{C}) \quad (42)$$

$$+ G(T, \mathbf{C} - \Delta C_i)) \quad (43)$$

The off-diagonals of this matrix are symmetric and solved for C_i and C_j where $i \neq j$ as:

$$\begin{aligned} \frac{\partial^2 G}{\partial C_i \partial C_j} = \frac{1}{\Delta C_i \Delta C_j} & (G(T, \mathbf{C} + \Delta C_i + \Delta C_j) \\ & - G(T, \mathbf{C} + \Delta C_i - \Delta C_j) \\ & - G(T, \mathbf{C} - \Delta C_i + \Delta C_j) \\ & + G(T, \mathbf{C} - \Delta C_i - \Delta C_j)) \end{aligned}$$

Lastly, the partial derivative of the entropy due to ΔC_i is solved as:

$$\frac{\partial S}{\partial C_i} = \frac{S(T, \mathbf{C} + \Delta C_i) - S(T, \mathbf{C} - \Delta C_i)}{2\Delta C_i} \quad (44)$$

Similarly to the isotropic expansion we can find the values for ΔC_i ($i = 1, 2, \dots, 6$) by determining the value of f that exceeds our energy cut-off. Values for f are shown in the following table:

9.3 1D-Anisotropic QHA

One dimensional is treated similarly to isotropic expansion, except V is replaced with λ , but all gradients are solved with a central finite difference approach. Based off of our definition λ at the lattice minimum structure is 0, so we have to re-define f as $f = \Delta\lambda$. We can then determine the most appropriate value of f by determine when our energy cut-off is met. For all four crystals we found that the the value of $f = 5 \times 10^{-3}$.

10 Euler and Runge-Kutta Step Sizes

A 4th order Runge-Kutta is sufficiently cheap and numerically stable to use for GradIso-QHA γ compared to a Euler method. We have carried out Euler and 4th order Runge-Kutta numerical methods for GradIso-QHA γ with varying step sizes. We have chosen to use the Grüneisen parameter because the results should be similar to GradIso-QHA and saves computational cost. In figure 14 the Gibbs free energy at 300K for both Euler and Runge-Kutta are compared for the varying number of steps between 0 and 300K to test the convergence of the results.

In all cases, $G(T = 300K)$ for Runge-Kutta is numerically indistinguishable for the varying number of steps used while the Euler approach converges on to the same result as the number of steps increases. With 12 Euler steps, the results still have not fully converged onto the Runge-Kutta results and the 12 step Euler approach is 3 \times more expensive than a single Runge-Kutta step. We have decided that a 4th order Runge-Kutta approach is the better choice and, with 3 steps from 0 to 300K (step size of 100K) having good performance. While similar results can be achieved with one step

size for Runge-Kutta, we want to be certain that we have converged on the isotropic volume that minimizes the free energy at intermediate points between 0 and 300K as well.

Due to the computational expense of the anisotropic gradient methods, we were unable to conduct a full Euler and Runge-Kutta analysis for anisotropic expansion. Since the results of isotropic expansion using the Runge-Kutta approach are stable, we have decided to perform anisotropic expansion with a three Runge-Kutta steps. If more steps were required, we stated so in the main paper.

11 Full Polymorph Free Energies

The plots in fig. 15 are the complete results for polymorph free energies summarized in the main paper. As stated in the main paper, the largest deviations in all methods are at 300 K. At all temperatures, the isotropic methods produce similar results and the free energy ranking $G_{HA} > G_{Iso.-QHA} \geq G_{Aniso.-QHA}$ holds true.

12 Analysis of Quasi-anisotropic Lattice Energies and Free Energies

Quasi-anisotropic QHA lowers the structures potential energy curve, $U(V)$, relative to isotropic expansion. However, the Gibbs free energy, $G(T > 0K, V)$, is not always lower. We found that the free energy for isotropic expansion could be lower in energy than the free energy curve found by quasi-anisotropic expansion, as the decrease in lattice energy compared to the isotropic case is compensated by an increase in vibrational energy. For all systems, we compared the free energies versus volume at 0 K and 300 K for the isotropic and quasi-anisotropic structures at varying volume fractions. Figures 16–19 shows the $U(V) + PV$ curves at 0 K (left) and the $G(V)$ curves at 300 K (right). At all volumes, except the lattice minimum structure, the constrained optimiza-

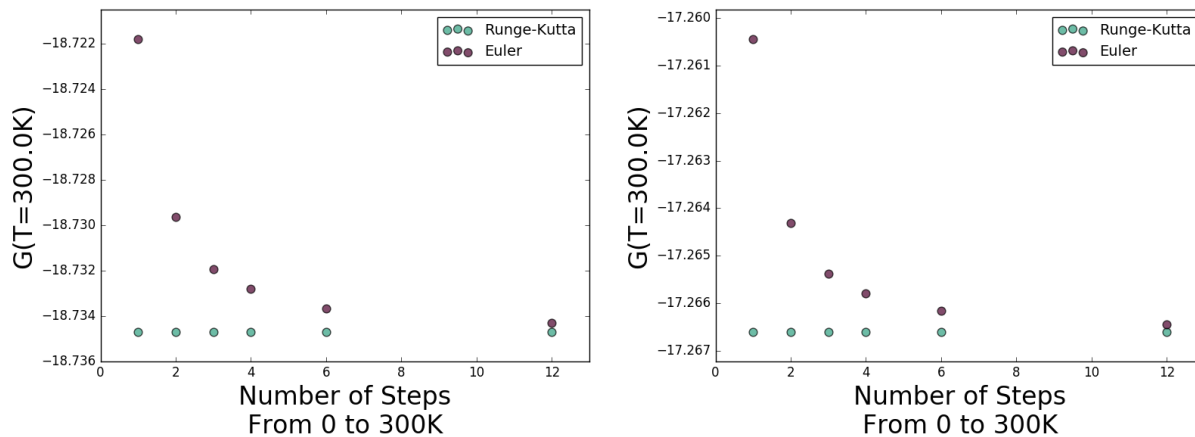


Figure 14: Comparison of converged Gibbs free energy at 300K for Euler and 4th order Runge-Kutta at varying step sizes for GradIso-QHA γ on piracetam form I (left) and III (right). There is little difference between 1 and 12 steps of Runge-Kutta, while Euler is greatly improved, but still does not converge on the Runge-Kutta Result.

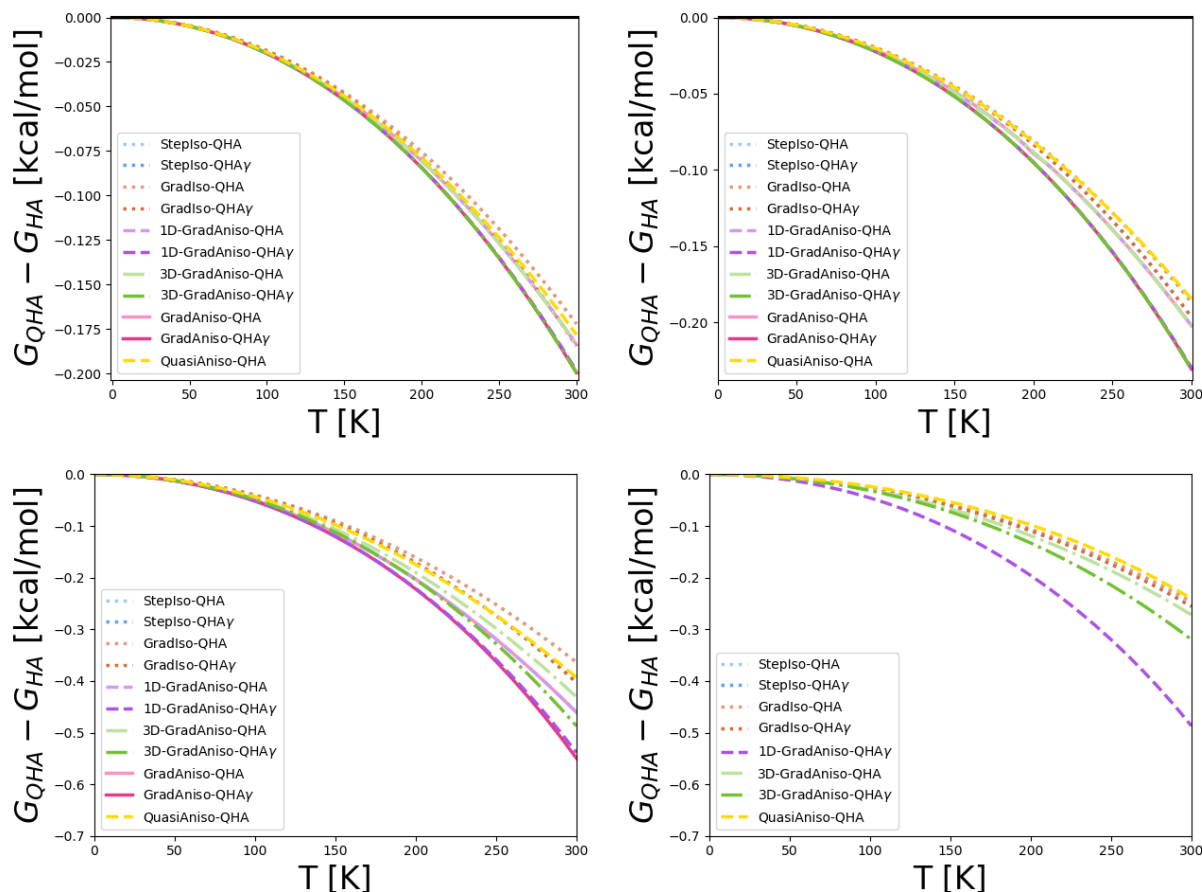


Figure 15: Deviations of the free energy of QHA methods from HA for resorcinol form α (top left), β (top right, and piracetam form I (bottom left) and III (bottom right). All methods show that the largest deviations occur at high temperatures and the relative rankings in methods are $G_{HA} > G_{Iso.-QHA} \geq G_{Aniso.-QHA}$.

tion properly reduces the potential energy by 0.0–0.1 kcal/mol relative to the isotropic structures. The figures on the right qualitatively show that the isotropic structures in many cases have lower free energy than the quasi-anisotropic structures.

13 Modifications to Tinker

All work in this paper was completed in Tinker 8.1 molecular modeling Package with modified code. We cannot re-distribute these modifications, but comment on the changes made. All modifications were to improve the accuracy and physical validity of the `vibrate` executable, which computes and returns the eigenvalues of the Hessian and mass-weighted Hessian. The eigenvalues of the mass-weighted Hessian are the crystals vibrational spectra in the form of wavenumbers.

Several of our systems from our previous work were outputting large negative wavenumbers, which is non-physical. For a properly geometry optimized structure, there should $3N - 3$ positive wavenumbers and 3 zero wavenumbers, where N is the number of atoms per cell. In the source code 'echarge2.f', which calculates the second derivative of the charge interactions, there is a comment noting that the reciprocal space contribution is neglected. We have implemented a central finite difference of the second derivative, using the correctly calculated first derivatives of the charge energy, to include the contribution to the reciprocal space. We verified the new vibrational spectra with `testhess`, a numeric solution of the Hessian, and have verified that the wavenumbers are all non-negative and have better agreement with the numeric solution than the previous analytic solution had.

14 Computing the Strain for the Grüneisen Parameter

In the main paper we discussed how we computed the strain, $\boldsymbol{\eta}$, between a deformed crystal \boldsymbol{C} and a reference crystal \boldsymbol{C}_0 . Here, we discuss

the derivation to get the equations in the main paper and how we remove any artificial rotation in present in the crystal.

14.1 Strain Treatment

For our 3×3 symmetric strain tensor, $\boldsymbol{\eta}$, we can compute a deformation gradient that is applied to the crystal lattice vectors. Since the strains applied to the lattice minimum crystal to minimize the free energy at $T > 0K$ are small, we have chosen to use the small strain definition to relate our desired strain with the deformation matrix, \boldsymbol{F} .

$$\boldsymbol{\eta} = \frac{1}{2}(\boldsymbol{F} + \boldsymbol{F}^T) - \boldsymbol{I} \quad (45)$$

We assume that angular momentum is conserved in the crystal matrix (i. e. no rotational component of \boldsymbol{F}), which implies that \boldsymbol{F} is symmetric and $\boldsymbol{F} = \boldsymbol{F}^T$. Our relationship between $\boldsymbol{\eta}$ and \boldsymbol{F} reduces to:

$$\boldsymbol{\eta} = \boldsymbol{F} - \boldsymbol{I} \quad (46)$$

$$\boldsymbol{\eta} + \boldsymbol{I} = \boldsymbol{F} \quad (47)$$

For a given crystal we can define the crystal tensor \boldsymbol{C} that is composed of the three vectors that describe the crystal space. If we wanted to determine the deformed crystal tensor, \boldsymbol{C}' , of a crystal deformed by strain $\boldsymbol{\eta}$, we would use the following relationship:

$$\boldsymbol{C}' = \boldsymbol{F}\boldsymbol{C} \quad (48)$$

$$\boldsymbol{C}' = (\boldsymbol{\eta} + \boldsymbol{I})\boldsymbol{C} \quad (49)$$

We can then re-arrange this to get resulting strain:

$$\boldsymbol{\eta} = \boldsymbol{C}\boldsymbol{C}_0^{-1} - \boldsymbol{I} \quad (50)$$

14.2 Removing Artificial Rotation

There is an artificial rotation in the computation of the strain in eq. 50 that must be removed before the strains can be used for the Grüneisen parameter. In eq. 50, both crystal tensors are upper triangle matrices, which will lead to an

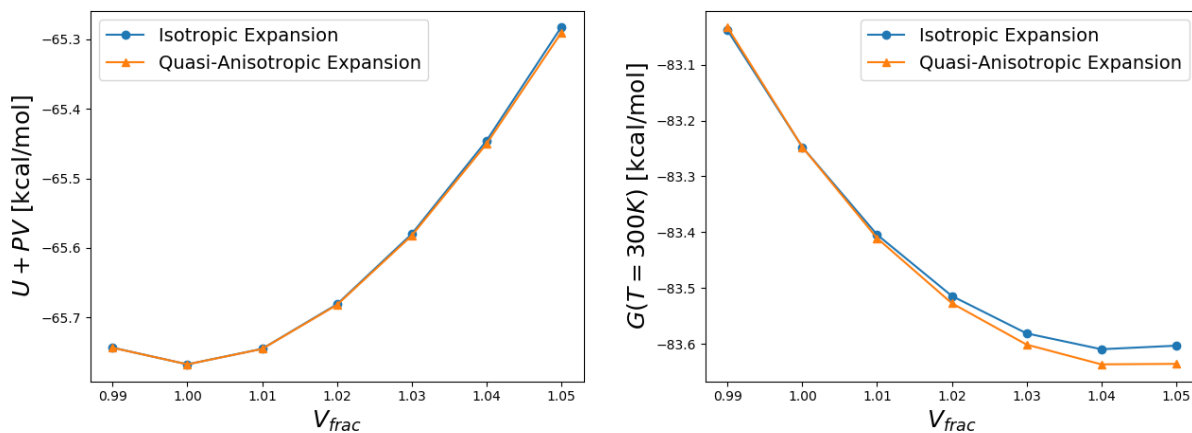


Figure 16: Lattice enthalpy (right) and Gibbs free energy at 300 K for piracetam form I for varying volume fractions using isotropic expansion and quasi-anisotropic expansion.

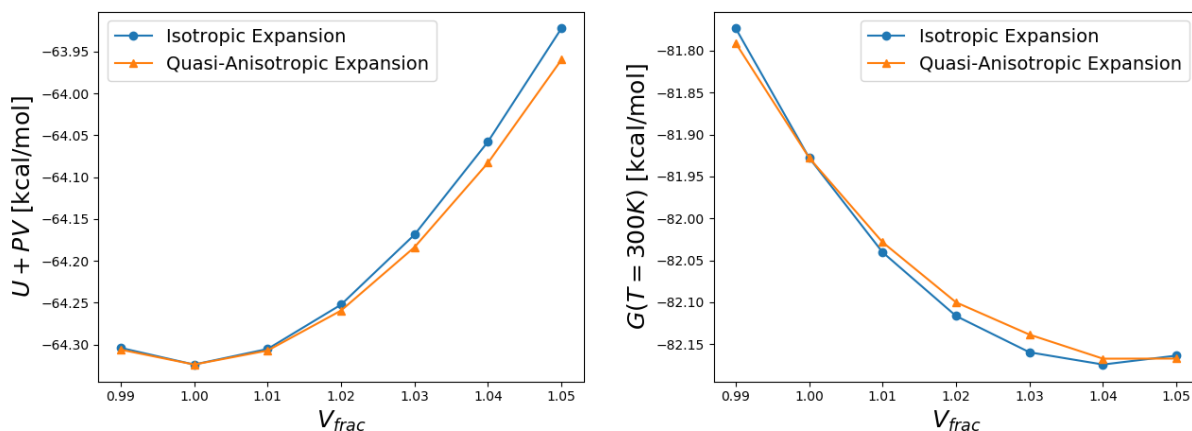


Figure 17: Lattice enthalpy (right) and Gibbs free energy at 300 K for piracetam form III for varying volume fractions using isotropic expansion and quasi-anisotropic expansion.

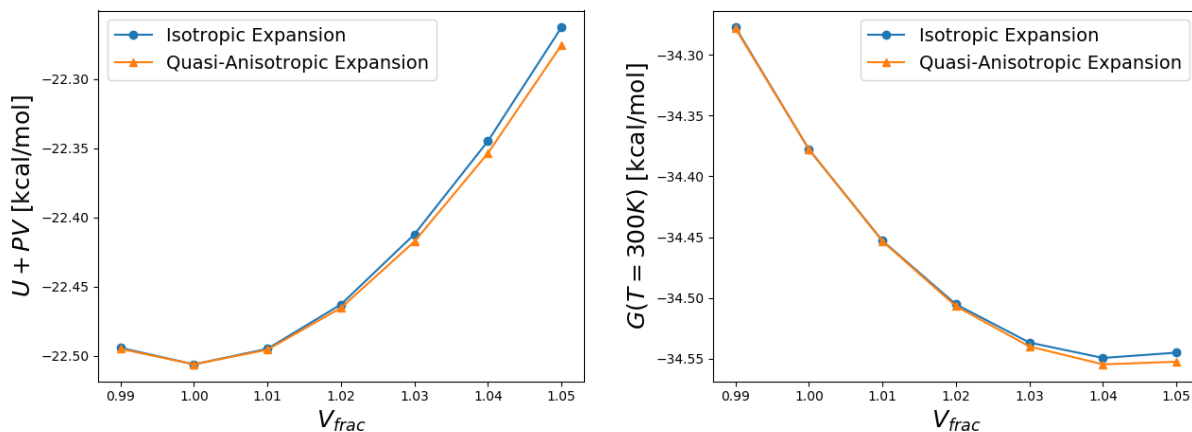


Figure 18: Lattice enthalpy (right) and Gibbs free energy at 300 K for resorcinol form α for varying volume fractions using isotropic expansion and quasi-anisotropic expansion.

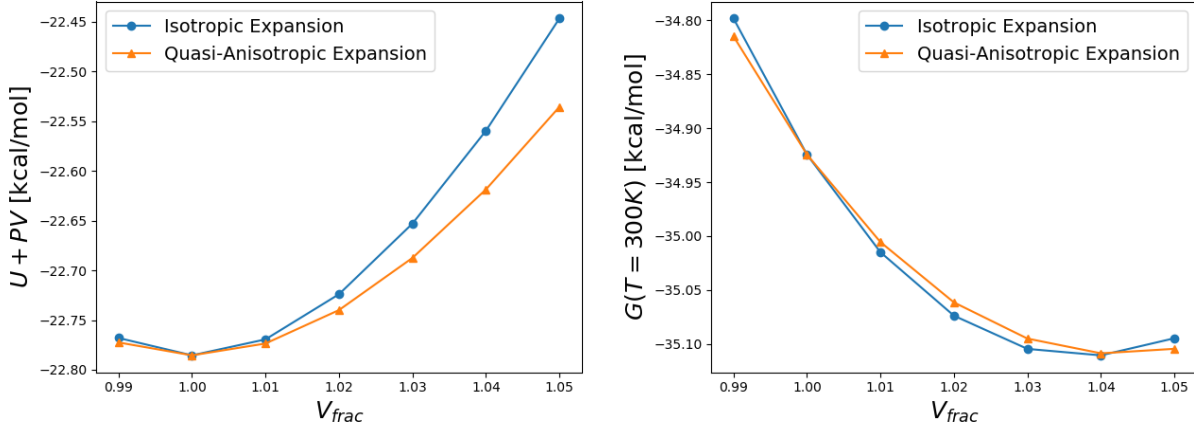


Figure 19: Lattice enthalpy (right) and Gibbs free energy at 300 K for resorcinol form β for varying volume fractions using isotropic expansion and quasi-anisotropic expansion.

asymmetric strain tensor. Since we are working with a bulk material in periodic boundary conditions, the rotation of the vectors in space will have zero effect on the potential or vibrational energy of the crystal. This artificial rotation between the two crystal tensors, \mathbf{C} and \mathbf{C}_0 , must be removed so we can compute the true strain between the two crystals. We use a decomposition method by Hoger and Carlson to determine the rotation and true strain applied to the crystal.⁴⁸

15 Matching Vibrational Modes

For all Grüneisen and the quasi-anisotropic approaches we are fitting each vibrational mode to a functional form. TINKER outputs the frequencies in numerical order, which leaves the possibility of mismatching between modes between two different structures. To assure that modes match before fitting our functional form we determine a weight between all eigenvectors and then use the Munkres python package to match each mode.

16 Constrained Volume Optimization Procedure

In the semi-anisotropic QHA method the lattice minimum structure is compressed and expanded to several volume fractions and then each expanded structure is optimized while constraining the volume. We use the `scipy.optimize.minimize` to perform the constant volume lattice minimization. We used the 'SLSQP' method, $tol = None$, $ftol = 10^{-6}$, and $eps = 10^{-4}$ all of which were optimized for computational speed and convergence within 10^{-8} kcal/mol.

To assure that the structure is at a minimum we used the method of Lagrange multipliers, where the Lagrange function to be minimized is shown in eq. 51.

$$\mathcal{L} = U(\mathbf{C}) - \lambda(V_0 - V(\mathbf{C})) \quad (51)$$

The derivative of \mathcal{L} with respect to each C_i ($i = 1, \dots, 6$) and λ should be zero when the crystal structure is optimized to the energy minimum at a given volume ($\mathcal{L}' = 0$). Due to numerical error, their values of \mathcal{L}' may be slightly non-zero. We checked the percentage of the derivatives of the optimized structure rela-

tive to the isotropic structure, shown in eq. 52.

$$\frac{\mathcal{L}'_{aniso.}}{\mathcal{L}'_{iso.}} \times 100\% \quad (52)$$

At 100% the structure is completely isotropic and 0% would be the lattice minimum structure for that volume. We found that all lattice parameters were $< 3\%$ for all optimized structures and the average value was 0.25%, which is within the range of accuracy for the results presented in this study.

References

- (1) Chemburkar, S. R.; Bauer, J.; Deming, K.; Spiwek, H.; Patel, K.; Morris, J.; Henry, R.; Spanton, S.; Dziki, W.; Porter, W.; Quick, J.; Bauer, P.; Donaubaue, J.; Narayanan, B. A.; Soldani, M.; Riley, D.; McFarland, K. *Org. Process Res. Dev.* **2000**, *4*, 413–417.
- (2) Bauer, J.; Spanton, S.; Henry, R.; Quick, J.; Dziki, W.; Porter, W.; Morris, J. *Pharm. Res.* **18**, 859–866.
- (3) Singhal, D.; Curatolo, W. *Adv. Drug Deliv. Rev.* **2004**, *56*, 335–347.
- (4) Haas, S.; Stassen, A. F.; Schuck, G.; Pernstich, K. P.; Gundlach, D. J.; Batlogg, B.; Berens, U.; Kirner, H.-J. *Phys. Rev. B: Condens. Matter Mater. Phys.* **2007**, *76*, arXiv: 0707.0461.
- (5) Giri, G.; Verploegen, E.; Mannsfeld, S. C. B.; Atahan-Evrenk, S.; Kim, D. H.; Lee, S. Y.; Becerril, H. A.; Aspuru-Guzik, A.; Toney, M. F.; Bao, Z. *Nature* **2011**, *480*, 504–508.
- (6) Reilly, A. M.; Cooper, R. I.; Adjiman, C. S.; Bhattacharya, S.; Boese, A. D.; Brandenburg, J. G.; Bygrave, P. J.; Bylsma, R.; Campbell, J. E.; Car, R.; Case, D. H.; Chadha, R.; Cole, J. C.; Cosburn, K.; Cuppen, H. M.; Curtis, F.; Day, G. M.; DiStasio Jr, R. A.; Dzyabchenko, A.; van Eijck, B. P.; Elking, D. M.; van den Ende, J. A.; Facelli, J. C.; Ferraro, M. B.; Fustimolnar, L.; Gatsiou, C.-A.; Gee, T. S.; de Gelder, R.; Ghiringhelli, L. M.; Goto, H.; Grimme, S.; Guo, R.; Hofmann, D. W. M.; Hoja, J.; Hylton, R. K.; Iuzzolino, L.; Jankiewicz, W.; de Jong, D. T.; Kendrick, J.; de Klerk, N. J. J.; Ko, H.-Y.; Kuleshova, L. N.; Li, X.; Lohani, S.; Leusen, F. J. J.; Lund, A. M.; Lv, J.; Ma, Y.; Marom, N.; Masunov, A. E.; McCabe, P.; McMahon, D. P.; Meekes, H.; Metz, M. P.; Misquitta, A. J.; Mohamed, S.; Monserrat, B.;

- Needs, R. J.; Neumann, M. A.; Nyman, J.; Obata, S.; Oberhofer, H.; Oganov, A. R.; Orendt, A. M.; Pagola, G. I.; Pantelides, C. C.; Pickard, C. J.; Podeszwa, R.; Price, L. S.; Price, S. L.; Pulido, A.; Read, M. G.; Reuter, K.; Schneider, E.; Schober, C.; Shields, G. P.; Singh, P.; Sugden, I. J.; Szalewicz, K.; Taylor, C. R.; Tkatchenko, A.; Tuckerman, M. E.; Vacarro, F.; Vasileiadis, M.; Vazquez-Mayagoitia, A.; Vogt, L.; Wang, Y.; Watson, R. E.; de Wijs, G. A.; Yang, J.; Zhu, Q.; Groom, C. R. *Acta Crystallogr., Sect. B: Struct. Sci.* **2016**, *72*, 439–459.
- (7) Motherwell, W. D. S.; Ammon, H. L.; Dunitz, J. D.; Dzyabchenko, A.; Erk, P.; Gavezzotti, A.; Hofmann, D. W. M.; Leusen, F. J. J.; Lommerse, J. P. M.; Mooij, W. T. M.; Price, S. L.; Scheraga, H.; Schweizer, B.; Schmidt, M. U.; Eijck, B. P. v.; Verwer, P.; Williams, D. E. *Acta Crystallogr., Sect. B: Struct. Sci.* **2002**, *58*, 647–661.
- (8) Lommerse, J. P. M.; Motherwell, W. D. S.; Ammon, H. L.; Dunitz, J. D.; Gavezzotti, A.; Hofmann, D. W. M.; Leusen, F. J. J.; Mooij, W. T. M.; Price, S. L.; Schweizer, B.; Schmidt, M. U.; Eijck, B. P. v.; Verwer, P.; Williams, D. E. *Acta Crystallogr., Sect. B: Struct. Sci.* **2000**, *56*, 697–714.
- (9) Day, G. M.; Motherwell, W. D. S.; Ammon, H. L.; Boerrigter, S. X. M.; Della Valle, R. G.; Venuti, E.; Dzyabchenko, A.; Dunitz, J. D.; Schweizer, B.; van Eijck, B. P.; Erk, P.; Facelli, J. C.; Bazterra, V. E.; Ferraro, M. B.; Hofmann, D. W. M.; Leusen, F. J. J.; Liang, C.; Pantelides, C. C.; Karamertzanis, P. G.; Price, S. L.; Lewis, T. C.; Nowell, H.; Torrisi, A.; Scheraga, H. A.; Arnautova, Y. A.; Schmidt, M. U.; Verwer, P. *Acta Crystallogr., Sect. B: Struct. Sci.* **2005**, *61*, 511–527.
- (10) Day, G. M.; Cooper, T. G.; Cruz-Cabeza, A. J.; Hejczyk, K. E.; Ammon, H. L.; Boerrigter, S. X. M.; Tan, J. S.; Della Valle, R. G.; Venuti, E.; Jose, J.; Gadre, S. R.; Desiraju, G. R.; Thakur, T. S.; van Eijck, B. P.; Facelli, J. C.; Bazterra, V. E.; Ferraro, M. B.; Hofmann, D. W. M.; Neumann, M. A.; Leusen, F. J. J.; Kendrick, J.; Price, S. L.; Misquitta, A. J.; Karamertzanis, P. G.; Welch, G. W. A.; Scheraga, H. A.; Arnautova, Y. A.; Schmidt, M. U.; van de Streek, J.; Wolf, A. K.; Schweizer, B. *Acta Crystallogr., Sect. B: Struct. Sci.* **2009**, *65*, 107–125.
- (11) Bardwell, D. A.; Adjiman, C. S.; Arnautova, Y. A.; Bartashevich, E.; Boerrigter, S. X. M.; Braun, D. E.; Cruz-Cabeza, A. J.; Day, G. M.; Della Valle, R. G.; Desiraju, G. R.; van Eijck, B. P.; Facelli, J. C.; Ferraro, M. B.; Grillo, D.; Habgood, M.; Hofmann, D. W. M.; Hofmann, F.; Jose, K. V. J.; Karamertzanis, P. G.; Kazantsev, A. V.; Kendrick, J.; Kuleshova, L. N.; Leusen, F. J. J.; Maleev, A. V.; Misquitta, A. J.; Mohamed, S.; Needs, R. J.; Neumann, M. A.; Nikylov, D.; Orendt, A. M.; Pal, R.; Pantelides, C. C.; Pickard, C. J.; Price, L. S.; Price, S. L.; Scheraga, H. A.; van de Streek, J.; Thakur, T. S.; Tiwari, S.; Venuti, E.; Zhitkov, I. K. *Acta Crystallogr., Sect. B: Struct. Sci.* **2011**, *67*, 535–551.
- (12) Price, S. S. L. *Acc. of Chem. Res.* **2009**, *42*, 117–126.
- (13) Nyman, J.; Day, G. M. *CrystEngComm* **2015**, *17*, 5154–5165.
- (14) Nyman, J.; Day, G. *Phys. Chem. Chem. Phys.* **2016**, *18*, 31132–31143.
- (15) Heit, Y. N.; Nanda, K. D.; Beran, G. J. O. *Chem. Sci.* **2015**, *7*, 246–255.
- (16) Boldyreva, E. V.; Shakhshneider, T. P.; Vasilchenko, M. A.; Ahsbahs, H.; Ucht-

- mann, H. *Acta Crystallogr., Sect. B: Struct. Sci.* **2000**, *56*, 299–309.
- (17) Varughese, S.; N.Kiran, M. S. R.; A.Solanko, K.; D.Bond, A.; Ramamurthy, U.; R.Desiraju, G. *Chem. Sci.* **2011**, *2*, 2236–2242.
- (18) Dolan, M. D.; Harlan, B.; White, J. S.; Hall, M.; Misture, S. T.; Bancheri, S. C.; Bewlay, B. *Powder Diffr.* **2008**, *23*, 20–25.
- (19) Wada, M. *J. Polym. Sci. B* **2002**, *40*, 1095–1102.
- (20) Bolotina, N. B.; Hardie, M. J.; Speer, R. L. J.; Pinkerton, A. A. *J. Appl. Crystallogr* **2004**, *37*, 808–814.
- (21) Dybeck, E. C.; Knig, G.; Brooks, B. R.; Shirts, M. R. *J. Chem. Theory Comput.* **2016**,
- (22) Ramrez, R.; Neuerburg, N.; Fernandez-Serra, M.-V.; Herrero, C. P. *J. Chem. Phys.* **2012**, *137*, 044502.
- (23) Filippini, G.; Gramaccioli, C. M.; Simonetta, M.; Suffritti, G. B. *Chem. Phys. Lett.* **1975**, *35*, 17–20.
- (24) Filippini, G.; Gramaccioli, C. M. *Acta Crystallogr., Sect. A* **1981**, *37*, 335–342.
- (25) Erba, A. *J. Chem. Phys.* **2014**, *141*, 124115.
- (26) Dovesi, R.; Erba, A.; Orlando, R.; ZicovichWilson, C. M.; Civalleri, B.; Maschio, L.; Rrat, M.; Casassa, S.; Baima, J.; Salustro, S.; Kirtman, B. *Wiley Interdiscip. Rev. Comput. Mol. Sci.* **2018**, *8*, e1360.
- (27) Erba, A.; Maul, J.; De La Pierre, M.; Dovesi, R. *J. Chem. Phys.* **2015**, *142*, 204502.
- (28) Erba, A.; Maul, J.; Civalleri, B. *Chem. Comm.* **2016**, *52*, 1820–1823.
- (29) Erba, A.; Shahrokhi, M.; Moradian, R.; Dovesi, R. *J. Chem. Phys.* **2015**, *142*, 044114.
- (30) Erba, A.; Maul, J.; Demichelis, R.; Dovesi, R. *Phys. Chem. Chem. Phys.* **2015**, *17*, 11670–11677.
- (31) Maul, J.; Santos, I. M. G.; Sambrano, J. R.; Erba, A. *Theor. Chem. Acc.* **2016**, *135*, 36.
- (32) Červinka, C.; O.Beran, G. J. *Phys. Chem. Chem. Phys.* **2017**, *19*, 29940–29953.
- (33) Day, G. M.; Price, S. L. *J. Am. Chem. Soc.* **2003**, *125*, 16434–16443.
- (34) Taylor, M.; Barrera, G. D.; Allan, N. L.; Barron, T. H. K. *Physica B* **1997**, *56*, 14380–14390.
- (35) Taylor, M.; Sims, C. E.; Barrera, G. D.; Allan, N. L.; Mackrodt, W. C. *Phys. Rev. B: Condens. Matter Mater. Phys.* **1999**, *59*, 6742–6751.
- (36) Dovesi, R.; Saunders, V. R.; Roetti, C.; Orlando, R.; Zicovich-Wilson, C. M.; Pascale, F.; Civalleri, B.; Doll, K.; Harrison, N. M.; Bush, I. J.; D’Arco, P.; Llunell, M.; Causà, M.; Noël, Y.; Maschio, L.; Erba, A.; Rerat, M.; Casassa, S. *CRYSTAL17 User’s Manual*. 2017.
- (37) Winkler, B.; Dove, M. T. *Phys. Chem. Miner.* **1992**, *18*, 407–415.
- (38) Iwanaga, H.; Kunishige, A.; Takeuchi, S. *J. of Mater. Sci.* **2000**, *35*, 2451–2454.
- (39) Das, D.; Jacobs, T.; Barbour, L. J. *Nat. Mater.* **2010**, *9*, 36–39.
- (40) Nath, P.; Plata, J. J.; Usanmaz, D.; Al Rahal Al Orabi, R.; Fornari, M.; Nardelli, M. B.; Toher, C.; Curtarolo, S. *Comput. Mater. Sci.* **2016**, *125*, 82–91.
- (41) Huang, L.-F.; Lu, X.-Z.; Tennessen, E.; Rondinelli, J. M. *Comput. Mater. Sci.* **2016**, *120*, 84–93.
- (42) Choy, C. L.; Wong, S. P.; Young, K. *Phys. Rev. B: Condens. Matter Mater. Phys.* **1984**, *29*, 1741–1747.

- (43) Gould, S.; Fernando, B.; Cherian, A.; Anderson, P.; Cruz, R. S.; Guo, E. *arXiv:1607.05447 [cs, math]* **2016**, arXiv:1607.05447.
- (44) Dybeck, E. C.; Abraham, N. S.; Schieber, N. P.; Shirts, M. R. *Cryst. Growth Des.* **2017**, *17*, 1775–1787.
- (45) Hairer, E.; Nørsett, S. P.; Wanner, G. *Solving Ordinary Differential Equations I: Nonstiff Problems*; Springer Science & Business Media, 2008; Google-Books-ID: F93u7VcSRyYC.
- (46) Ponder, J. W.; Richards, F. M. *J. Comput. Chem.* **1987**, *8*, 1016–1024.
- (47) Giannozzi, P.; Baroni, S.; Bonini, N.; Calandra, M.; Car, R.; Cavazzoni, C.; Davide Ceresoli,; Chiarotti, G. L.; Cococcioni, M.; Dabo, I.; Corso, A. D.; Gironcoli, S. d.; Fabris, S.; Fratesi, G.; Gebauer, R.; Gerstmann, U.; Gougousis, C.; Anton Kokalj,; Lazzeri, M.; Martin-Samos, L.; Marzari, N.; Mauri, F.; Mazzarello, R.; Stefano Paolini,; Pasquarello, A.; Paulatto, L.; Sbracciacia, C.; Scandolo, S.; Sclauzero, G.; Seitsonen, A. P.; Smogunov, A.; Umari, P.; Wentzcovitch, R. M. *J. Phys.: Condens. Matter* **2009**, *21*, 395502.
- (48) Hoger, A.; Carlson, D. E. *Quarterly of Applied Mathematics* **1984**, *42*, 113–117.